DEVELOPMENT OF TERSOFF POTENTIAL MODELS TO STUDY SILICON DOPANT ACTIVATION IN INDIUM GALLIUM ARSENIDE

A Thesis

Presented to the Faculty of the Graduate School

of Cornell University

In Partial Fulfillment of the Requirements for the Degree of

Master of Science

by

Cheng-Wei Lee

August 2014

ABSTRACT

A parameterization of the Abell-Tersoff potential is presented for all pairwise interactions of silicon atoms with each of the elemental components comprising InGaAs. That is, Tersoff models are provided for Si-In, Si-Ga and Si-As. Data obtained using *ab initio* pseudopotential calculations (DFT+GGA) were used as the reference information against which the Tersoff parameters were fitted, since experimental data are unavailable for the Si-X systems considered here. These sets of Tersoff parameters are optimized to describe the structural and elastic properties of the mostly theoretical alloys Si-As, Si-Ga and SI-In. We demonstrate the transferability of these parameters by partially predicting the defect formation energies of extrinsic point defects of Si across ternary InGaAs alloys with different local configurations. Comparison is made to a newly created DFT/GGA database of defect formation energies, showing that correct trends can be reproduced by the Tersoff models, given sensitive adjustments to a Tersoff model parameter, μ_{ij}.

BIOGRAPHICAL SKETCH

Cheng-Wei Lee was born on the 20th of August, 1989, at a small town in Tainan City (used to be Tainan County), Taiwan to San-Tai Lee and Chin-Feng Liang. The author had spent his first 15 years in this lovely small town until he started his high school in Tainan First Senior High and moved to Tainan City. His general interest in natural science rooted from the memorable playtime spent on the beautiful village field. During his time in high school, he survived several competitive challenges to finally make it to the top university in Taiwan, National Taiwan University (NTU), and received a B.S. degree in Materials Science and Engineering. His interests in science and engineering was further fostered in NTU and started to focus on multi-scale aspects of the materials. He found a way to observe the world beyond daily experience intriguing and the ability to describe the phenomenon from the atomic scale fascinating. This made him to start a new adventure in pursuing the knowledge of computational materials science (CMS). He ended up in Cornell University and joined the computational group led by Prof. Paulette Clancy. His germinating research interest in CMS was fostered in this free, independent and mutually supportive group. He received a M.S. degree in Cornell and will continue his further adventure at the University of Illinois at Urbana-Champaign as a Ph.D. student.

致 親愛的父母及家人和在身邊陪伴和支持我的 Jocelyn

ACKNOWLEDGMENTS

First of all, I would like to thank Prof. Paulette Clancy for her guidance and encouragement throughout my M.S. degree. Her strict attitude toward the results and the way of presentation also helps me build up the essential skills in communication. Most of all, her optimistic attitude toward the hard questions helped me conquer the obstacles of the project. I would also like to thank Dr. Binit Lukose for his constant help in teaching me how to use several useful tools in UNIX system and his time for enlightening discussion of the project.

Second, I would like to thanks Prof. Michael O. Thompson for insightful questions and informative suggestions during the project meetings. His "physical sense" questions always make me think deeper into the problems and learn a lot from them. I would also like to thanks all the experimental group members in the joint project for sharing insights and details of the experiments and analysis.

Third, I would like to thank all the members in Prof. Clancy's group. Their whole-hearted help throughout my time in the group helped me survive the steep learning curve of computational materials science. Their informative questions and suggestions help me learn beyond the project I was working on.

Last, but not least, I would like to thank Dr. Michelle Johannes (NRL) and Prof. Richard Hennig for discussions regarding the formulation of the defect formation energy. I would also like to thank Drs. Phil Oldiges and Pranita Kulkarni (IBM) for sharing their insights regarding InGaAs.

This research was supported by the Semiconductor Research Corporation's Global Research Collaboration and is closely related to the focus of SRC contract number 2012-VJ-2272. Computing resources are provided by the Cornell Institute for Computational Science and Engineering, supported by equipment donations from Intel and capital equipment funding from

Cornell’s Center for Materials Research, an NSF-funded MRSEC (DMR-1120296). Part of the XSEDE computing time was kindly shared by Prof. Richard Hennig (Dept. of Materials Science and Engineering at Cornell).

TABLE OF CONTENTS

LIST OF FIGURES

LIST OF TABLES

CHAPTER 1

Introduction

1.1 Importance of $In_{0.53}Ga_{0.47}As$ as a channel material

Due to efforts to continue on Moore's law for the past few decades, the size of the transistor has been scaled down in order to integrate more transistors into the chip. However, several challenges have arisen:

1. Physical challenges: As the size of the transistor reached nanometer scale, tunneling effects began to dominate resulting in current leakage.
2. Materials challenges: Mostly regarding the dielectric and wiring materials as the scaling continues.
3. Power and Thermal challenges: As the number of transistors per unit area goes up, the power consumption and thermal dissipation becomes a serious issue.
4. Lithography challenges: As the characteristic length of the device becomes smaller than the wavelength of light, it is harder to maintain the resolution.
5. Economical challenges: Due to rising costs, it has become unaffordable to continue along Moore's law.

$In_{0.53}Ga_{0.47}As$ has attracted a lot of attention due to its lower power consumption and better performance. As mentioned in a 2010 presentation by Intel's Director of Technology Strategy, Paolo Gargini, "the inclusion of III-V materials is a 2015 transistor option could deliver either

three times the performance of silicon at the same power consumption, or deliver the same performance as silicon at one-tenth the power consumption [1].”

1.2 Properties of $In_{0.53}Ga_{0.47}As$

$In_{1-x}Ga_xAs$ is a solid solution of GaAs and InAs [2] and therefore shares the zincblende structure. The specific composition x=0.47 is chosen to have lattice-match with InP which works as the substrate due to its much better accessibility compared to InGaAs. The relations between composition and lattice constant/energy gap are shown in Figures 1 and 2, respectively, on the next page [2][3]. The electrical properties of $In_{1-x}Ga_xAs$ are listed in Table 1.

Table 1. Basic electrical properties of channel materials at 295K

Material	Si	Ge	InAs	GaAs	$In_{0.53}Ga_{0.47}As$
e^-/h^+ Mobility (cm^2/V-s)	~1,400/ ~380	~3,900/ ~1900	~40,000/ ~500	~8,500/ ~400	~10,000/ ~250
Band gap (eV)	1.1	0.66	0.354	1.424	0.75
Gap type	indirect	indirect	direct	direct	direct
Lattice const.(Å)	5.431	5.646	6.05	5.6535	5.869

Figure 1. Lattice parameters of InGaAs vs. the GaAs fraction

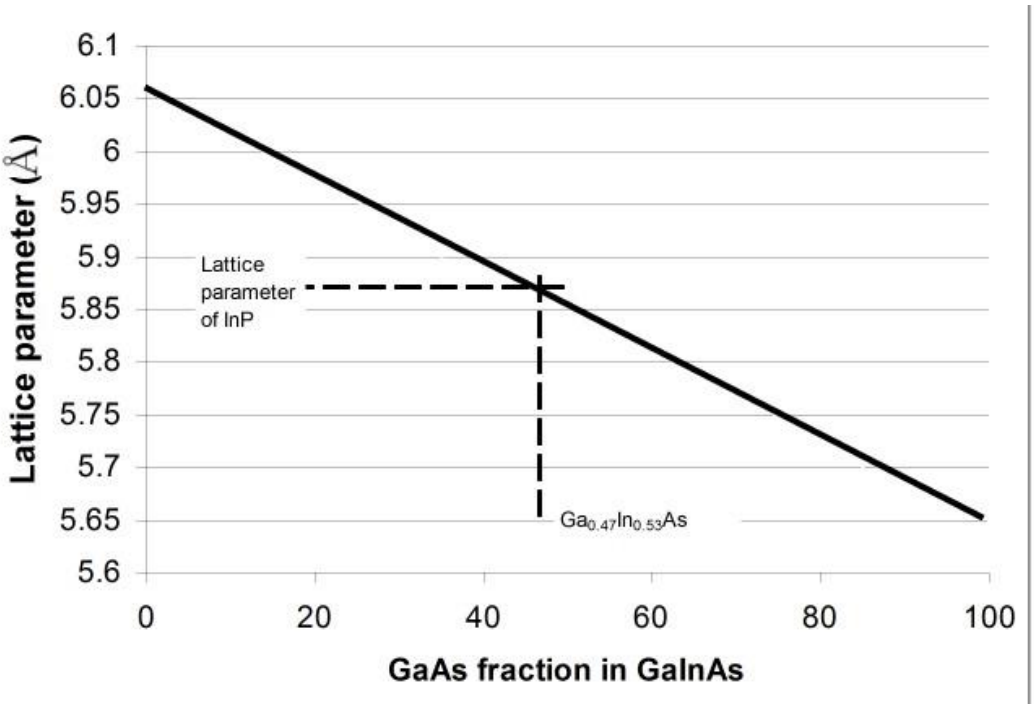

Figure 2. Energy gap vs. Ga composition

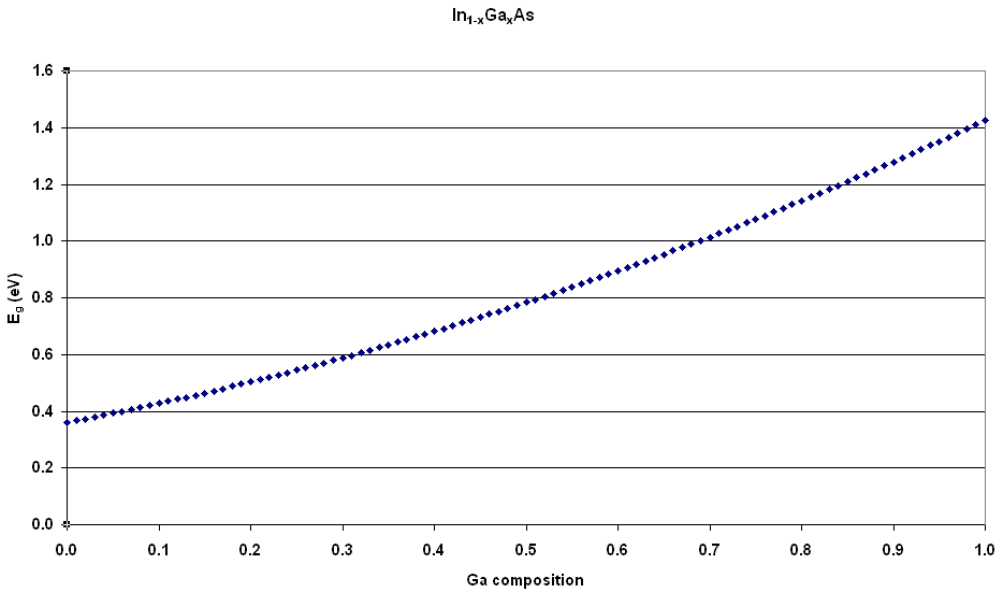

In addition to their application as channel materials, the direct band gap feature of III-V materials has made them desirable materials for photo-related applications such as photo-detectors, photovoltaics and lasers.

1.3 $In_{0.53}Ga_{0.47}As$ as a potential channel material beyond Si-based CMOS

The scaling of power consumption of Si-CMOS stopped at 130 nm and the supply voltage remained at around 1.0 eV. The major reasons are (1) kT/q does not scale and (2) the leakage currents are set by the threshold voltage (V_T). The variation of threshold voltage, mostly caused by random dopant fluctuations (RDF), also affects the processing. In addition to optimizing the energy to performance relation for the Si-CMOS, the other idea is to find the new channel material. As shown in Table 1, $In_{0.53}Ga_{0.47}As$ has approximately 7~8 times higher electron mobility compared to silicon which can enhance the performance and reduce the power consumption at for the same voltage supply as Si. However, $In_{0.53}Ga_{0.47}As$ has a lower hole mobility compared to Si. Therefore, Ge, with its substantially higher hole mobility, is proposed to be a suitable p-type channel material to be combined with InGaAs as n-type to form beyond-CMOS devices.

1.4 Challenges for III-V materials, especially $In_{0.53}Ga_{0.47}As$

Despite the promising potential for $In_{0.53}Ga_{0.47}As$, there are three major challenges:

1. Poor quality of the high-k/III-V interface
2. Junction technology

3. Hetero-integration on Si

In the past, III-V materials have had difficulties competing with Si-based CMOS due to the absence of a low defect density native oxide. The defect states at the interface between the channel and the gate oxide, which could not be passivated efficiently, resulted in pinning of the Fermi-level. Being unable to adjust the Fermi level causes difficulties in processing and the functionality of the device. These issues have become less critical with the shift to high-k dielectric materials, such as hafnium oxide. Recently, improvements in the interface quality have reopened the possibility of III-V materials as viable alternatives to silicon for high density microelectronics. Indeed, these materials have already begun to be incorporated into the 2012 ITRS (International Technology Roadmap for Semiconductors) [4]

A key process in device fabrication from doped InGaAs materials involves the ability to optimize the activation of dopants, especially the commonly used n-type dopant, silicon, using a suitable annealing process. While experimental investigations of this system of Si-doped InGaAs are still relatively rare, preliminary results have shown that the activation of Si dopants is unexpectedly difficult within a temperature range that will not break the integrity of the interface (usually ~600 ℃): silicon has been reported not to move readily within the InGaAs host matrix at higher temperatures, as evidenced using SIMS [5]. Since a higher dopant activation rate is essential for lower channel resistance, this unexpectedly low activation of Si in InGaAs is a problem. Understanding the origins of the low dopant activation is the motivation for this computational study.

Although not the focus of this study, hetero-integration on a silicon platform is a further challenge facing the adoption of III-V systems. For III-V materials to be considered seriously as an alternative to Si-based systems, it will be necessary to utilize the existing powerhouse of Si-based manufacturing technology.

1.5 Aim of this work

This dopant activation issue was computationally approached in two ways. First, since Si dopants need to occupy the cationic lattice site (In or Ga) if they are to be electron contributors, first principles (*ab initio*) methods were used to determine if it is more energetically (thermodynamically) likely for Si to reside at substitutional cation sites, rather than at anion sites. Second, since there is a driving force for Si to occupy cation sites for some processing conditions, we hypothesized that the migration of Si atoms is impeded by certain disadvantageous local atomic environments, such that Si cannot reach desirable cation sites, and hence explaining the lack of dopant diffusion and activation. We investigated this by calculating the total energies of all possible atomic configurations surrounding Si atoms within a second nearest neighbor distance. Given that we are considering a ternary host matrix, the number of possible unique arrangements of neighbors is large. Since first principles methods remain too computationally expensive to solve such combinatorial problems, we turn to the availability of semi-empirical models, such as the Tersoff potential model, to describe the interactions between pairs of atoms. The much higher computational efficiency of such models allows us to undertake larger-scale molecular simulations containing thousands of atoms that can more realistically capture the

transport of Si dopants in the InGaAs matrix. Fortunately, suitable Tersoff models exist for the III-V materials, both the elemental systems (In-In [6], Ga-Ga [6], As-As [6]) and all the unlike pairs of atom types, *e.g..,* Ga-As [6]). However, there are no Tersoff models for the Si-X interactions (where X = In, Ga, or As). Hence we develop and test suitable Tersoff models in this thesis.

1.6 Thesis Outline

In this thesis, I will begin by describing the theoretical background of the methods used here, namely Density Functional Theory and the Tersoff potential model. The parameter fitting procedure for the Tersoff models and the determination of material properties is provided in chapter 3. A discussion of the results of the DFT database and the best parameter sets of Tersoff models are given in chapter 4. The conclusions we reached regarding the appropriateness of the Tersoff models will be described in chapter 5. Lastly, I will briefly describe the next steps for studying dopant activation in InGaAs given the models I developed in Chapter 6

CHAPTER 2

Theoretical background

2.1 Introduction to Density Functional Theory (DFT)

2.1.1 Background of First Principles Calculations

For the material properties concerned in this study, such as bulk structural properties and defect formation energy, a physical model constituted by a set of nuclei and electrons interacting via Coulomb forces is able to predict the values generally within 1% error. This can be theoretically achieved by solving the Many-Body Schrodinger Equation (MBSE) [7]. However, given that current computational resources restrict the consideration of no more than three particles, a number of approximations are required in order to make this first principles approach practical.

2.1.2 Born-Oppenheimer Approximations

One of the commonly used approximations in solid-state physics is the Born-Oppenheimer approximation which decouples the movements of electrons from nuclei. This approximation is based on the fact that nuclei move much slower than electrons; therefore, from the point of view of the electrons, the nuclei are basically static. This is generally true in this study since only

ground-state properties are considered. This approximation transforms the wavefunction of the position of nuclei and electrons into the wavefunction of electron with frozen nuclei. The interactions among nuclei then become the constant, simplifying the calculation. However, acquiring the electronic structure by solving the Many-Body Schrodinger Equation with an electron Hamiltonian is still beyond the reach of modern computational power.

2.1.3 Hartree-Fock Method

In order to solve the MBSE problem after the Born-Oppenheimer approximation is applied, one common approach used in the field of quantum chemistry is the Hartree-Fock (HF) Approximation [8]. Briefly, the all-electron wavefunction is approximated by one Slater determinant (since the electron is a fermion) that contains a single-electron wavefunction. This is done using the idea of a self-consistent field combined with the method of variational optimization and trial wave functions. However, the HF method does not take into account the electron correlation, *i.e.*, the repulsion of electrons. But it does account for the electron exchange by inclusion of the Fock theory.

2.1.4 Post Hartree-Fock Method

Several methods were proposed to deal with the electron correlation problem of the Hartree-Fock method. In brief, this involved three directions:

First, treat the electron correlation term as a perturbation of the Fock operator; usually the Møller-Plesset perturbation theory [9] is used.

Second, expand the all-electron wave function in terms of linear combinations of Slater determinants, such as the configuration interaction (CI) method [10][11].

Last, use a statistical approach and treat all the electrons explicitly, such as the Quantum Monte Carlo (QMC) method [12][13].

These approaches increase the accuracy of the calculation but also they also increase the computational cost.

2.1.5 Density Functional Theory (DFT)

In solid-state physics, the mainstream approach of first principles calculation is the so-called density functional theory (DFT) which treats both electron exchange and correlation approximately. Density Functional Theory is based on two central theorems due to Hohenberg and Kohn [14] and the Kohn-Sham equation [15] which treats the many-body problem by using the idea of employing a functional and assuming the electron charge density as the key variable. In other words, the properties of the many-body system are rewritten in terms of a functional of spatially dependent electron density. Only the concepts of the theory will be briefly reviewed in the following section. More detailed reviews of all the details of DFT can be found in [16]

Hohenberg-Kohn Theorem I:

This theorem states that the energy of an electronic system is a functional of the electron density, *i.e.*, E=E [ρ(r)]. This idea greatly reduces the many-body problem of N electrons with 3N spatial coordinates to only 3 spatial coordinates of the electron density. This theorem also means that there is a one-to-one correlation between the external potential (in most case from the nuclei) and the electron density. That is, given an external potential, there is only one density while given the density of electron, there is only one corresponding potential.

Hohenberg-Kohn Theorem II:

The energy functional is defined in this theorem and it also proves that the ground state can be found by minimizing the energy functional by variational method, only the results are shown below:

$$E_0 = \min E[\rho(r)]$$

where

$$\frac{\partial E[\rho(r)]}{\partial \rho(r)} = 0$$

E_0 is the ground state energy of the system. $E[\rho(r)]$ is the energy functional of the electron density function $\rho(r)$.

Kohn-Sham theory:

This theory states that the density can be expanded in a different way without losing the generality. Therefore, the many-body problem can now be mapped onto a single particle Schrodinger-like equation if all the terms are written as the functionals of density. Every term in the energy functional can now be almost written in terms of density except for the exchange correlation terms into which all the unknown functionals are placed.

2.1.6 The electron exchange-correlation functional

No one really knows how to write this exchange correlation functional in terms of the electron density, but we can learn from studying the simplest imaginable system: a homogeneous electron gas (HEG). Due to its simplicity, all the terms we placed into the exchange-correlation functional can now be solved exactly at some limits. This is done by solving the system piece by piece as shown in Figure 3.

Figure 3. Piecemeal solution of homogeneous electron gas.

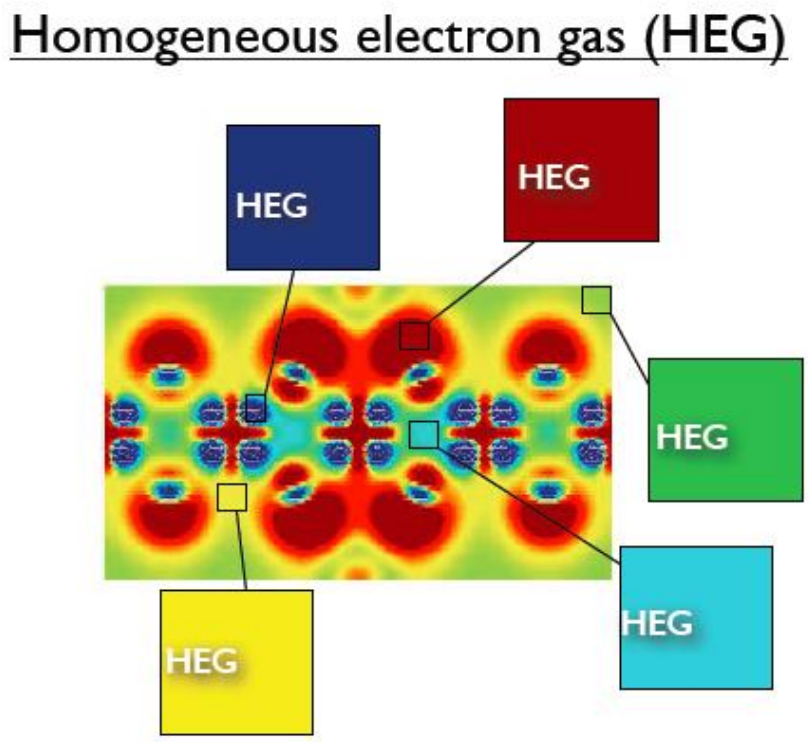

As you can see in Figure 3, the electron density is homogeneous at some limits, the area away from these limits is acquired by interpolation. This approach is called the "local density approximation "(LDA).

In order to improve the limitation of LDA to homogeneous-like systems, a gradient term in the density is added. Therefore, the exchange-correlation functional depends not only on density, but also on its gradient. This method is called the "generalized gradient approximation" (GGA).

2.1.7 Limitation of LDA/GGA

The accuracy of LDA/GGA inevitably depends on how close the system of interest is to a homogeneous electron gas system. The GGA method is chosen in this study due to its generally improved predictive ability, especially the prediction of the bulk properties of purely theoretical compounds. There is no systematic study dealing specifically with the performance of GGA to represent the ternary II/V material, InGaAs, not to mention the Si-X interactions of interest here, but a benchmark can still be acquired from the general study of GGA itself.

2.1.8 Solving the single-particle Hamiltonian

In order to solve the Hamiltonian constructed above, a basis set for single-particle wave functions is needed. There are generally two choices, each with their own advantages and disadvantages:

(1) Atomic orbitals: This is a particularly suitable choice close to the nuclei, but a poor one when mimicking the plane-wave-like nature in solids. A very large number of atomic orbitals are required to reproduce plane waves. Also the derivatives are difficult to calculate and their Fourier transform is slow to evaluate.

(2) Plane waves: This is a very appropriate choice for solids, but a poor one close to the nuclei. A very large number of plane waves is needed to reproduce the oscillations of

deep electrons. However, the derivatives are straightforward to compute and the Fourier transform is fast.

One way to solve this dilemma is by combining the two approaches. This approach is called the augmented plane wave (APW). The atomic orbitals are used within a certain radius from the nuclei and the plane waves are used beyond this radius. This "full-potential" is accurate, but still too expensive to use to represent the nuclei region.

The idea of a pseudopotential was then proposed using the fact that core electrons are inactive and do not affect the valence electrons. Therefore, since the oscillation of the core electrons is irrelevant to the properties being considered, we can smooth out the oscillations as illustrated in Figure 4, while keeping the total charge constant. Once the oscillations are smoothed out, the potential can now be reproduced by a reasonable number of plane waves which is efficient to calculate for the Fourier transforms and easy to take derivatives.

The last challenge of solving the single-particle Hamiltonian is that there are approximately 10^{23} electrons in the solids making it infeasible to calculate. Fortunately, in this thesis we will be dealing with bulk crystalline solids which are periodic. Therefore, this problem can be approached by choosing the minimum representation of the system, *i.e.*, the unit cell.

Figure 4. Comparison between the full potential (shown in blue) and the pseudopotential (shown in red). The oscillations of core electrons, *i.e.*, the region smaller than r_c, are smoothed out by the pseudopotential

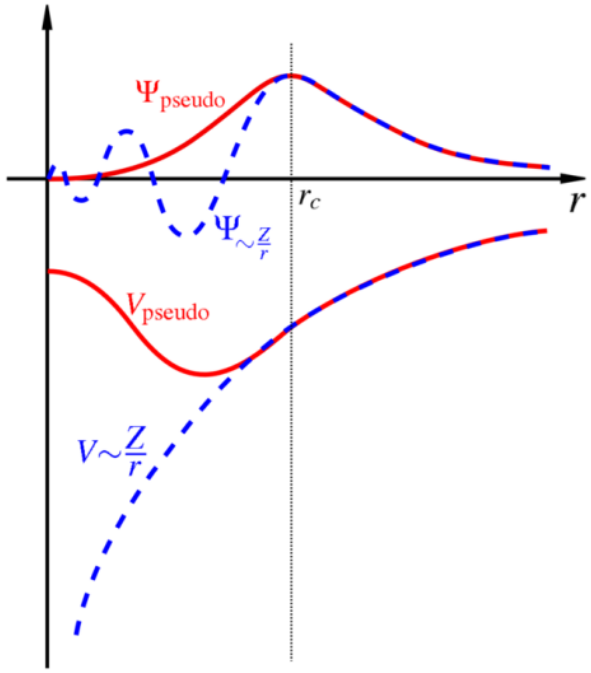

2.1.9 Bloch theorem and k-mesh

If periodic boundary conditions are employed, the wave function can be written as a plane wave function multiplied by a function with lattice periodicity, and this is the basic idea of the Bloch theorem. Since the Bloch function is a periodic function, for each k, it can be expanded into Fourier components. However, it is impractical to have infinite terms for the expansion. Therefore a convergence test with respect to total energy is required to make the calculations efficient while maintaining accuracy.

However, a wavefunction is needed for each k and the number of k values is infinite. Fortunately, the k points are confined within a space and regularly spaced. Therefore, instead of an integral over space, we can make a mesh of k points and use a sum, as long as the mesh is dense enough

to give an unchanging integral. The k-mesh is generated by using the Monkhorst-Pack algorithm [17]. It should be noticed that the density of the k-mesh depends on the size of the unit cell. The smaller the unit cell, the larger the k-space, requiring a denser k-mesh.

In practical terms, we need to undertake a convergence test with respect to the total energy for the kinetic energy which is directly related to the size of the expansion and the k-mesh density. The cutoff criteria used here is 5meV/atom, which is relatively stringent for the properties considered in this work. The results for the systems in this study are shown in Table 2.

2.1.10 Conclusions regarding Density Functional Theory

The Hamiltonian of the many-body problem is greatly simplified by writing each term as functionals of electron density which have proved to be valid when written as the single-particle Schrodinger equation. The exchange and correlation terms are made exact by the local density approximation and further revised by the generalized gradient approximation.

The overwhelming large number of single-particle Hamiltonians is simplified by the periodic nature of crystalline solids. But a convergence test on the kinetic energy and density of the k-mesh are required in order to make sure that the total energy remains unchanged.

Although a DFT approach has been made practical due to the theorems mentioned here and the significant increases in computational powers in recent years, the scale of system size and computational time is still limited, in practice, to the consideration on a single processor of about 100-200 atoms and relaxation on the order of picoseconds.

Table 2. The results of convergence tests on the kinetic energy and density of various k-meshes for a 2x2x2 supercell, unless otherwise noted.

system	Cutoff kinetic energy (Ry)	k-mesh
In	70	1x1x1* /11x11x11⊥
Ga	50	1x1x1* /6x6x6⊥
As	30	1x1x1* /10x10x10⊥
Si	30	1x1x1* /8x8x8⊥
Si-As	30	5x5x5
Si-Ga	50	2x2x2
Si-In	60	2x2x2
GaAs	50	4x4x4
InAs	60	4x4x4
InGaAs	50	4x4x4

* Isolated atoms with an extremely large supercell

⊥ 1x1x1 unit-cell for the naturally stable crystal structure.

2.2 Semi-empirical Tersoff potential model

2.2.1 Introduction of the Tersoff potential model

The Tersoff potential model was originally developed for Si [18][19] and later extended to Ge and SiC by Tersoff [20]. Tersoff models fall into the category of "bond order" potentials originally suggested by Abell, in which the two-body potential depends on the environment of the neighboring atoms. Like the Stillinger-Weber model, the Tersoff potential was developed for covalently bonded systems.

Extension of the Tersoff model to describe III-V alloys has been reasonably widespread: Smith developed Tersoff parameters for the simulation of atomic collisions in GaAs [21]. The first set of Tersoff parameters for AlAs was developed by Sayed *et al.* [22]. Extension to InAs was made by Ashu for studies of ion bombardment [23], and further modified by Nordlund [24]. A comprehensive set of Tersoff parameters for many III-V materials of technological interest was developed by Migliorato *et al.* for application of quantum dot optoelectronics [25]. Tersoff parameters for In-As and Ga-As were also developed by Hammerschmidt [6], which are used for our application here. Of more direct importance to our interest in doped InGaAs materials, Detz and Strasser recently tested Tersoff models for InGaAs, InAlAs, and GaAsSb for their ability to reproduce elastic properties, as well as predict bulk and shear moduli [26].

2.2.2 Description of the Abell-Tersoff Potential Model

The Abell-Tersoff family of interatomic potential models has given rise to several different forms since it was first presented by Tersoff [27][18]. All of these forms write the total energy of the system as a sum over all the interactions of atom i to its neighboring atom j, as shown below: (By definition, the cohesive energy can be derived by dividing by the number of atoms and multiplying by two):

$$E = \frac{1}{2}\sum_i \sum_{i \neq j} f_{ij}^c\left(r_{ij}\right)\left[V_{ij}^R\left(r_{ij}\right) - B_{ij}\left(r_{ij}\right)V_{ij}^A\left(r_{ij}\right)\right] \quad (1)$$

where E is the total energy of the system; f_{ij}^{c} is the cut-off function; $V_{ij}^{R}$is the repulsive potential energy, while V_{ij}^{A} is the attractive potential energy; $B_{ij}$is the bond-order term. The attraction term is multiplied by the bond-order term, which takes into account the particle's neighboring environment and coordination number.

The pair potential, V_{ij}, in equation 1 includes terms describing the repulsive, V^{R}_{ij} and attractive interactions, V^{A}_{ij}, and uses a form akin to a Morse potential with one additional adjustable variable, S_{ij} , which controls the relationship between bond energies and distances. The form of the repulsive and attractive terms is given by:

$$V_{ij}^{R}(r_{ij}) = \frac{D_{ij}}{S_{ij}-1}\exp\left[-\beta_{ij}\sqrt{2S_{ij}} * \left(r_{ij} - R_{ij}^{0}\right)\right] = A \times exp(-\lambda_1 \times r) \qquad (2)$$

$$V_{ij}^{A}(r_{ij}) = \frac{S_{ij}D_{ij}}{S_{ij}-1}\exp[-\beta_{ij}\sqrt{2/S_{ij}} * (r_{ij} - R_{ij}^{0})] = B \times exp(-\lambda_2 \times r) \qquad (3)$$

The first and second mathematical formalisms given in equations 2 and 3 clarify the difference between the relationship used by Hammerschmidt [6] and Tersoff [18], respectively. In equations 2 and 3, D_{ij} is the equilibrium diatomic energy that controls the depth of the potential energy well; the β_{ij} term controls the width of the well. R_{ij}^{0} is the equilibrium diatomic distance. The bond-order term (eqn. 4) shows an inverse relation to (1+ $\gamma_{ij}\zeta_{ij}$). ζ_{ij} is sometimes called the pseudo-coordination, constituted by the number of neighbors, k, to atom i ($k \neq i$, eqn. (5)), a bond angle term given in g(θ) (eqn. (6)) and a bond stiffness term in the exponential term (eqn. (6)). γ_{ij} is an additional term to adjust the bond-order term. The g_{ik} parameter essentially controls the

resistance to bend by adjusting the relative numbers of c_{ik} ,$d_{ik}$and h_{ik}, while the exponential term controls the resistance to stretch by adjusting u_{ik} and m_{ik}. δ_{ik} adjusts the strength of the contribution from neighboring atoms. h_{ik} is defined as $\cos\theta_0$ which is the reference angle between the ij and ik bonds.

$$B_{ij}(r_{ij}) = \{1 + [\gamma_{ij}\zeta_{ij}(r_{ij})]^{n_{ij}}\}^{-\frac{1}{2n_{ij}}} \quad (4)$$

$$\zeta_{ij}(r_{ij}) = \sum_{k\neq i,j} f_{ik}^{c}(r_{ik}) * g_{ik}(\theta_{ijk}) * \exp\{[u_{ik}(r_{ij} - r_{ik})]^{m_{ik}}\} \quad (5)$$

$$g_{ik}(\theta_{ijk}) = \delta_{ik}[1 + \frac{c_{ik}^2}{d_{ik}^2} - \frac{c_{ik}^2}{d_{ik}^2 + (h_{ik} - \cos\theta_{ijk})^2}] \quad (6)$$

$$f_{ij}^{c}(r_{ij}) = \begin{cases} 1, & r_{ij} - R_{ij}^{c} \leq -D_{ij}^{c} \\ \frac{1}{2}\left[1 - \sin\left(\frac{\pi}{2}\frac{r_{ij} - R_{ij}^{c}}{D_{ij}^{c}}\right)\right], & |r_{ij} - R_{ij}^{c}| > D_{ij}^{c} \\ 0, & r_{ij} - R_{ij}^{c} \geq D_{ij}^{c} \end{cases} \quad (7)$$

The cut-off function is used to ensure a smooth truncation beyond the cut-off point of the potential to zero to avoid impulses in the force and includes first nearest neighbors only. There is no interaction between atom i and atoms that are further than a distance R_{ij}+D_{ij} away from one another.

2.2.3 Parameterization procedure of Tersoff potential model

While there is no standard procedure for fitting parameters involved in the formulation of a force field or interatomic potential model, there are several necessary steps that are involved:

The first requirement, in the absence of experimental data, is to create a comprehensive and reliable reference database of properties of the system being modeled. In the case of the Si-X interactions, no experimental data are available since Si-Ga and Si-In are theoretical compounds and Si-As has rarely been studied experimentally [28]. In such cases, it is necessary to create a reference database using first principles methods, principally Density Functional Theory (DFT) and Generalized Gradient Approximations (GGA) [29], as described in section 2.1.

The second component involves the fitting procedure itself. We follow the approach used previously by Biswas *et al.* [30] and by Tersoff [18] and use a non-linear least squares fit procedure (here, a Levenberg-Marquardt algorithm using Genplot [31]).

The last step involves the validation of the parameters. Initially, we compared the results of the Tersoff model-generated results against the DFT reference database. Then in order to check the transferability of the best parameter set to properties that match our particular research interests, we also predict properties that were *not* included in the first fitting process. We chose to predict the defect formation energy due to its critical role in dopant activation, which was a primary motivation for us to create these Tersoff models. These three steps will be explained in details for the following three sub-sections.

2.2.4 Creation of *ab initio* database

The quality of the parameters obtained for a given force field or interatomic potential model depends to a considerable extent on the quality of the reference database. For a bond-order-type interatomic potential model, like the Tersoff model, having as many crystal structures as possible as part of the reference database is desirable. However, some approximations should be also considered. Since the form of Tersoff model used in this work takes into account only first nearest neighbors (1nn) and symmetry bonding, *i.e.*, an A-B bond is the same as a B-A bond, only crystal structures that conform to this limitation were included in the reference database. Cubic structures (such as simple cubic, diamond, ZnS, NaCl, and CsCl) are symmetric and can be well described by a 1nn-based model; therefore, they are widely used for Tersoff parameter fitting. The first two structures (simple cubic and diamond) are mostly used for pure elements and are not included in this work. Other common crystal structures for compound materials, such as wurtzite, NiAs, h(exagonal)-BN structures were also considered, but only h-BN passed our screening: Wurtzite behaves the same as ZnS under the 1nn approximation; NiAs has an asymmetric nature for its local bonding. Therefore, we are left with consideration of ZnS, NaCl, CsCl, and h-BN as our reference database for the parameter fitting process.

2.2.5 Parameter determination

For the most general and commonly used form of the Tersoff model, there are 14 parameters. Of these fourteen, four of them can be found from experimental data: D_{ij} and R_{ij}^{0} are the diatomic

binding energy and equilibrium length, respectively. Two others, β_{ij} and S_{ij} , can be determined if enough experimental data are available [32]: β_{ij} can be determined if both D_{ij} and the ground state frequency are known. S_{ij} can be determined from the Pauling relation [32]. However, in this case, since there are no experimental data, these four parameters remain free but should acquire values that do not lead to unphysical predictions, such as overly large diatomic binding energies or equilibrium bond lengths. This additional freedom to set four more variables may help us find a better fit to the reference data; but it can also result in multiple sets of parameters, whose relevant merit will have to be evaluated. The n_{ij} parameter is set to 1 to be in agreement with the second-order momentum approximation. γ_{ij} is an additional adjustable parameter, but was set to 1 in this work following the procedure of Albe et al. [32]. Parameter m_{ij} can be set to either 1 or 3 in LAMMPS; it was set to 1 in this work, following Hammerschmidt's procedure [6].

Parameters governing the cut-off functions for the Tersoff models are not included in the systematic fitting process, since determining the appropriate cut-off values to use is complicated. Most prior work has followed Tersoff's original approach and assumed that the cut-off is made at a distance corresponding to the inclusion of first nearest neighbors for each crystal structure. Albe *et al.* took a different approach [32]: they chose to reproduce the melting point as the metric in determining a suitable value for the cut-off; but even this group did not include the cut-off in their fitting procedure. This work follows the original Tersoff method, and does not include the cut-off value in the fitting process. Here, the cut-off radius was chosen to lie between the equilibrium bond lengths of first and second nearest neighbors of each crystal structures, *i.e.*, ZnS, NaCl, CsCl, h-BN, and further determined by inclusion of the relaxed bond length of Si

dopant to its first nearest neighbors at all the defect position of interest. All the equilibrium bond lengths were acquired from our DFT calculations.

Some of the parameters were fitted under certain constraints to prevent unphysical results. For example, h, which is defined as $\cos\theta_{ijk}$, should be bigger than -1 and smaller than 1. S_{ij} should not equal 1; otherwise repulsion and attraction terms will result in values of infinity and the fitting process will fail. The remaining parameters (γ_{ij}, c_{ij}, d_{ij}, μ_{ij}) are adjustable with no constraints. However, we found during the fitting process that the parameter μ_{ij}, which is mostly related to the h-BN structure, was extremely important in determining the defect formation energy, which is a prime concern to our proposed application for these models. The parameter μ_{ij} controls the resistance to stretch and the relative bond length for the connecting bonds. It is not only the μ_{ij} values of the binary Si-X models that matter, but also those of In-As/Ga-As alloys. Therefore, in order to be compatible with the existing In-Ga-As Tersoff model, the μ_{ij} values were separately adjusted so that they reproduced the correct trend in a set of defect formation energies that targeted Si-X interactions in a variety of different environments, but sacrificing the h-BN structure.

2.2.6 Validation of parameters

The results of the fitting to create viable parameter sets are shown in Table 3. The first set of parameters, named "parameter set 1 (ps.1)", not only fits bulk properties well, but also provided a qualitatively good prediction of the DFT results for defect formation energies.

Table 3: Parameter sets for Si-X pairwise interactions

	Si-As (ps.1)	Si-As (ps.2)	Si-Ga*	Si-In*
D_{ij}(eV)	4.79841	4.3381	3.124428	3.3719795
R_{ij}^{0}(Å)	2.13339	2.0978	2.1973155	2.3111975
S_{ij}	1.913203	1.26936	1.2005	1.3574872
β_{ij}(1/Å)	1.082611	1.13142	1.2789162	1.17268
δ_{ij}	0.271506	0.0952155	0.05845635	0.1356779
c_{ij}	1.640876	0.342903	0.53355	0.1811664
d_{ij}	0.9159	0.531886	0.655665	0.3842507
h_{ij}	-0.10111	-0.170953	-0.358167	-0.2569319
μ_{ij}(1/Å)	-1.19500	-0.415	-1.295	1.15
γij	1.0	1.0	1.0	1.0
nij	1.0	1.0	1.0	1.0
mij	1.0	1.0	1.0	1.0
R_{ij}^{c}(Å)	3.2	3.2	3.2	3.3
D_{ij}^{c}(Å)	0.1	0.1	0.1	0.1

* Parameters for Si-Ga and Si-In are identical for ps. 1 and ps. 2.

Initially, we compared the results of the Tersoff model-generated results against the DFT reference database that we created and which was described above; see Table 4. Since the three ps.1 Tersoff parameter sets for Si-Ga, Si-In and Si-As that are given in Table 3 are each a best fit

across all cubic crystal structures, it is not guaranteed that they will reproduce the *ab initio* data from which they were generated. Parameter sets are invariably a compromise that improve the reproduction of one structure often worsen the reproduction of properties for another structure.

As a case in point, we provide (in Table 3) an alternative parameter set, named "parameter set 2 (ps.2)", with the same Si-Ga and Si-In interactions, but a different Si-As interaction. We found it was only necessary to modify the Si-As potential model to obtain a good fit to defect formation energies. The Si-As potential of ps.2 was a broad-fit to all four crystal structures selected above (*i.e.*, including h-BN) instead of only cubic crystals in ps.1. Anticipating the results that follow, we shall show that the ps.2 models provide better values of the defect formation energies in *interstitial* environments than ps.1, but at the expense of failing to reproduce the DFT-generated trends that show comparable formation energies for cationic and anionic *substitutional* defects.

Table 4. Equilibrium bulk properties of Si-X interactions from *ab initio* calculations (DFT/GGA) and from the Tersoff models

Si-As

Crystal structure	E_{coh}(eV) GGA/ps.1/2	Bond length (Å)	B (GPa)
ZnS	4.70/4.71/4.71	2.48/2.47/2.44	49/49/56
NaCl	4.88/4.85/4.86	2.61/2.65/2.64	93/74/82
CsCl	4.51/4.53/4.57	2.81/2.81/2.84	77/87/94
ZnO*■	4.85/4.71/4.71	2.43/2.47/2.44; 2.75/2.47/2.44	60/49/56
NiAs■	4.84/4.67/4.77	2.63/2.67/2.65	84/89/87
h-BN*⊥	4.86/4.68/4.78	2.51/2.54/2.52; 2.60/2.63/2.61	71/56/68

* wurtzite and h-BN are hexagonal structures which are characterized by both a- and c-directions

■ results for ZnO and NiAs are included although they were not used in the fitting ⊥ The c/a value of 1.03582 for Si-As was kept constant during relaxation

Si-Ga

Crystal structure	E_{coh}(eV) GGA/ps.1&2	Bond length (Å)	B (GPa)
ZnS	3.85/3.85	2.45/2.44	76/58
NaCl	3.84/3.84	2.62/2.65	64/79
CsCl	3.77/3.79	2.81/2.80	61/102
ZnO	3.82/3.85	2.47/2.44; 2.40/2.44	62/58
NiAs	3.93/3.91	2.67/2.64	69/92
h-BN⊥	3.81/3.69	2.42/2.49; 2.89/2.71	62/63

⊥ The c/a value of 1.08846 for Si-Ga was kept constant during relaxation

Si-In

Crystal structure	E_{coh}(eV) GGA/ps.1&2	Bond length (Å)	B (GPa)
ZnS	3.51/3.51	2.64/2.65	37/32
NaCl	3.54/3.53	2.82/2.86	47/57
CsCl	3.48/3.48	3.02/3.01	66/72
ZnO	3.50/3.51	2.66/2.65; 2.60/2.65	48/32
NiAs	3.64/3.56	2.88/2.85	46/65
h-BN⊥	3.49/3.47	2.63/2.66; 3.03/3.00	50/45

⊥ The c/a value of 1.117 for Si-In was kept constant during relaxation

2.3 Materials properties determination

2.3.1 Structural properties

Cohesive energies and lattice constants were calculated by minimizing the energy of the system of interest (*e.g.*, a given crystal structure) using Beeman's algorithm and the Wentzcovitch Lagrangian as implemented in Quantum Espresso [33]. The cell constants are allowed to change during the minimization. The total energies of isolated atoms were calculated by having a huge cell size to prevent interaction among atom and its mirror images. The bulk modulus is calculated by fitting the equation of state to that for a Murnaghan formulation [34]. The results are shown in Table 4.

2.3.2 Defect formation energy

Compared to pure elements, the defect formation of multi-component system is chemical potential-dependent. However, the chemical potential is not directly calculable. We can only assign a range for the chemical potential of each element within which the system will have a particular thermodynamic phase. In our case, this will be a homogeneous solid solution of InAs and GaAs.

The general form of the defect formation energy can be written as:

$$\Omega_D = E_D + Q_D \times \mu_e - n_{In} \times \mu_{In} - n_{Ga} \times \mu_{Ga} - n_{As} \times \mu_{As} - n_{Si} \times \mu_{Si} \quad (8)$$

where E_D is the total energy of the InGaAs system with a Si dopant. Q_D is the charge on the dopant. μ_e is the chemical potential of an electron, also known as the Fermi level with E_v (valence band edge) equal to 0. n_i is the number of atoms of element i in the supercell. μ_i is the chemical potential of element i, which depends on its environment.

The defect formation energy of a ternary compound depends on the chemical potential. Computationally, we take this into account by minimizing eqn. (8) with the following constraints (eqns. 9-15) in order to produce the lowest Gibbs free energy.

$$\mu_{In} + \mu_{Ga} + 2\mu_{As} = {\mu_{InGaAs_2}}^{B} \tag{9}$$

$$\mu_{In}^{B} + \mu_{Ga}^{B} + 2\mu_{As}^{B} - \mu_{InGaAs_2} = \Delta H_f^{InGaAs_2} \tag{10}$$

$$\mu_{Ga} + \mu_{As} \leq {\mu_{GaAs}}^{B} \tag{11}$$

$$\mu_{In} + \mu_{As} \leq {\mu_{InAs}}^{B} \tag{12}$$

$$\mu_{Si} + \mu_{As} \leq {\mu_{SiAs}}^{B} \tag{13}$$

$$\mu_e \leq E_g \tag{14}$$

$$\mu_i \leq \mu_i^B \tag{15}$$

The superscript ‘B’ in all the equations refers to the chemical potential of bulk materials, *i.e.*, the chemical potential of the corresponding materials with naturally stable crystal structures.

For eqns. (11-14), the upper limits are set by the chemical potential of the naturally stable crystal structures of each element. The chemical potential of each element in InGaAs alloy should be smaller than the values of their stable crystal structures or they will precipitate. In eqn. (15), it is not necessary to have the Fermi level within the band gap, but generally we are more interested in this range.

Combining eqns. (9) and (15) gives us:

$$\mu_{Ga}^{B} - \Delta H_f^{InGaAs_2} \leq \mu_{Ga} \leq \mu_{Ga}^{B} \tag{16}$$

$$\mu_{In}^{B} - \Delta H_f^{InGaAs_2} \leq \mu_{In} \leq \mu_{In}^{B} \tag{17}$$

$$\mu_{As}^{B} - \Delta H_f^{InGaAs_2} \leq \mu_{As} \leq \mu_{As}^{B} \tag{18}$$

As we can see in eqns. 16-10, the chemical potentials of Ga, In, and As are related by the formation energy ($\Delta H_f^{InGaAs_2}$) and the chemical potential of bulk InGaAs (μ_{InGaAs_2}). In order to discuss how the defect formation energy depends on the chemical potential of In, Ga, and As, the following two terms are defined and assigned a specific range using eqns. 10 and 16-18 [35][36][37][38] to compare cation-rich conditions to anion-rich conditions, as well as In-rich to Ga-rich conditions.

$$\Delta\mu = (\mu_{In} + \mu_{Ga} - 2\mu_{As}) - (\mu_{In}^{B} + \mu_{Ga}^{B} - 2\mu_{As}^{B}),$$

where

$$-\Delta H_f^{InGaAs_2} \leq \Delta\mu \leq \Delta H_f^{InGaAs_2} \tag{19}$$

and

$$\delta\mu = (\mu_{In} - \mu_{Ga}) - (\mu_{In}^{B} - \mu_{Ga}^{B}), \tag{20}$$

where

$$-\frac{1}{2}(\Delta H_f^{InGaAs_2} - \Delta\mu) \leq \delta\mu \leq \frac{1}{2}(\Delta H_f^{InGaAs_2} - \Delta\mu) \quad (21)$$

Taking these two terms into consideration and rewriting eqn. (8), we have:

$$\Omega_D = E_D{}' + Q_D \times \mu_e - \frac{1}{4}(n_{In} + n_{Ga} - n_{As})\Delta\mu - \frac{1}{2}(n_{In} - n_{Ga}) - n_{Si} \times (\mu_{Si} - \mu_{Si}{}^{Bulk}) \quad (22)$$

$$E_D{}' = E_D - \frac{1}{2}\left(n_{In} - \frac{n_{As}}{2}\right) \times (\mu_{In}{}^{B} - \mu_{As}{}^{B})$$

$$-\frac{1}{2}\left(n_{Ga} - \frac{n_{As}}{2}\right) \times (\mu_{Ga}{}^{B} - \mu_{As}{}^{B})$$

$$-\frac{1}{4}(n_{In} + n_{Ga} + n_{As}) \times \mu_{InGaAs_2}{}^{B}$$

$$-\frac{1}{4}(n_{In} - n_{Ga}) \times (\mu_{In}{}^{B} - \mu_{Ga}{}^{B})$$

$$-n_{Si}\mu_{Si}{}^{B} \quad (23)$$

where E_D' is independent of the chemical potential and can readily be calculated. Now, we are in a position to compare the defect formation energy under different processing conditions, *i.e.*, we can calculate the chemical potential to see which defect is more stable under certain processing conditions. It should be noticed that we should not confuse the atmospheric environment mentioned here with the local environment of Si dopants in an InGaAs alloy.

2.3.3 Calculation of the total energy of InGaAs alloy with Si dopant

In order to simulate the defect in crystalline solids by plane-wave-based DFT, we need to use a large enough supercell to prevent the interactions among the defect and all the mirror defects around it, as illustrated in Figure 5, since the supercell is repeated in three dimensions indefinitely. Therefore, we need to conduct a convergence test to describe how the total energy of the system with defects and the size of supercell are related. The results are shown in Table 5, and the defects will be described later. For the defect formation energy calculations in this work, we chose a 64-atom supercell as the trade-off between accuracy and efficiency. The error in the defect formation energy, according to this table, is estimated to be around 0.1 eV for a substitutional defect and 0.2 eV for interstitial defects.

There are two ways to calculate the total energy of crystalline solids with a defect. The one used in this work involves a full relaxation of the pure crystalline solids first. Then, after the defect is incorporated into the solids, the system is internally relaxed with constant lattice parameters from the previous fully relaxation kept constant. On the other hand, we can also directly fully relax the system of solids that include a defect. However, in general, the latter approach requires a bigger supercell to converge, therefore it is more expensive to compute.

Figure 5. Schematic representation of the periodic nature of plane-wave-based DFT and the possible interactions between the defect (brown) and its mirror images (purple)

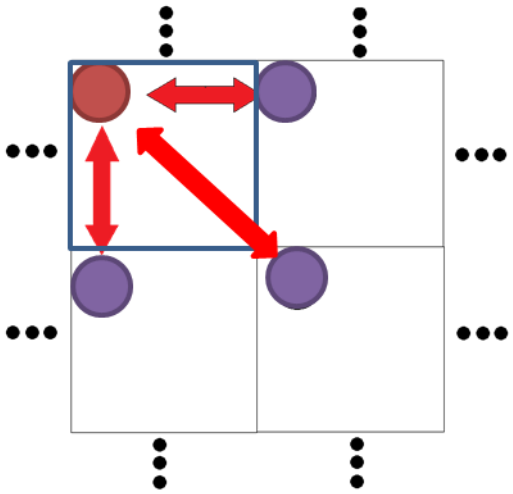

Table 5. Convergence test on the cell size effect of the defect formation energy (DFT)

Defect*	16-atom (eV)	64-atom (eV)	128-atom (eV)
$(Si_{Ga})^0$	1.20	0.97	0.91
$(Si_{In})^0$	0.95	0.51	0.46
$(Si_{As})^0$(Ga-rich)	0.71	0.69	0.66
$(Si_{As})^0$(In-rich)	0.87	0.90	0.89
$(Si_{T1})^0$	2.96	3.02	2.82
$(Si_{T2})^0$ (Ga-rich)	3.21	2.97	2.76
$(Si_{T2})^0$ (In-rich)	3.45	3.23	3.04
$(Si_{H})^0$ (Ga-rich)	3.12 (stable)	T2 (Ga-rich)	T2 (Ga-rich)
$(Si_{H2})^0$ (In-rich)	2.78 (stable)	T2 (In-rich)	T2(In-rich)

*This table was discussed in the (Ga,In)-rich condition, with $\boldsymbol{\mu_{Si} = \mu_{si}^{B}}$. The Fermi level plays no role for the neutral uncharged defect. Configuration 1 for the InGaAs matrix was used for the results shown in this table.

In this study, the ultimate goal is develop a semi-empirical model that can find the most probable local environment around a Si dopant in InGaAs. Therefore, this model should be able to predict the correct energy differences, or at least the right trend, among different local environments and across different defect types. This is tested by comparing the extrinsic defect formation energies of a single Si dopant in InGaAs alloys which exhibit different In/Ga arrangements around the Si atom. Three representative configurations are shown in Figure 6. The defects studied in this work were generally divided in three categories: (1) cationic substitutional defects (2) anionic substitutional defects (3) T1 and T2 interstitial defects. A cation substitutional defect is defined as a Si dopant atom substituted for either a Ga or an In atom located on a cationic lattice site. An anionic substitutional defect is defined as a Si dopant atom substituted for an As atom on an anionic lattice site. A T1 interstitial defect is defined as a Si dopant atom occupying a tetrahedral interstitial site and surrounded by anions (As, in this study). A T2 interstitial defect is defined as a Si dopant atom occupying a tetrahedral interstitial site and surrounded by cations (Ga or In, in this study).

Figure 6. Description of the three configurations chosen to test the ability of the Tersoff models to represent different arrangements of In/Ga atoms

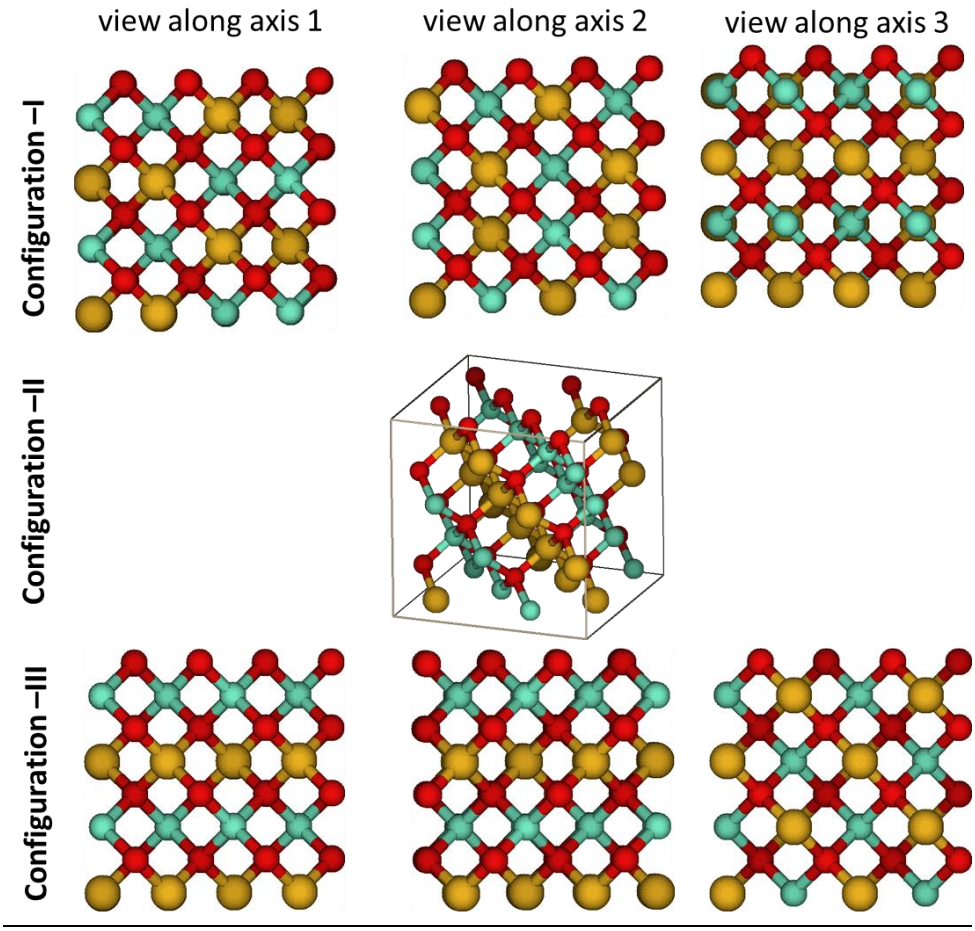

* Red: As; light green: Ga; yellow: In

Configuration 1 has either ABAB or AABB patterns along the (001) direction on the cationic atom plane and is the random arrangement of In/Ga that we studied

Configuration 2 has In/Ga arranged in alternating layers along the (111) direction

Configuration 3 has In/Ga arranged in alternating layers along the (001) direction

2.3.4 Micro-segregation of In/Ga atoms at the second nearest neighbor of Si

In order to test the hypothesis that the local environment around a Si atom will affect its preference for a lattice site, we chose to explore the most extreme versions of the nature of the 12 second nearest neighbors of the Si atom. That is, we considered systems in which the second nearest neighbors of the Si atom were either all Ga or all In atoms. The remainder of the InGaAs matrix was a random alloy of In and Ga cation sites. Thus, the total numbers of Ga and In atoms are kept constant at 50 In and 50 Ga per 100 As atoms. This is represented in Figure 7 as the pathway II to IV. We chose configuration 1 (Config.1) of InGaAs for this study since it has the most randomly arranged set of In/Ga atoms and this configuration has the lowest energy among all the configurations used in this study. Thus using Config. 1 prevents introducing strain energy into the system from ordering the In and Ga atoms.

Figure 7. Decoupling the effects of strain energy and defect formation energy using a set of pathways that explore the net effect of micro-segregation. Situation I describes the randomly arranged pure InGaAs alloy displayed by configuration 1. Situation II has one randomly chosen Ga site replaced by a Si atom. Situation III describes the local micro-segregation of In/Ga at the 2nn sites of a (randomly chosen) chosen Ga site. Situation IV has the chosen Ga site (in Situation III) replaced by Si with the 2nn occupied by all In or Ga atoms.

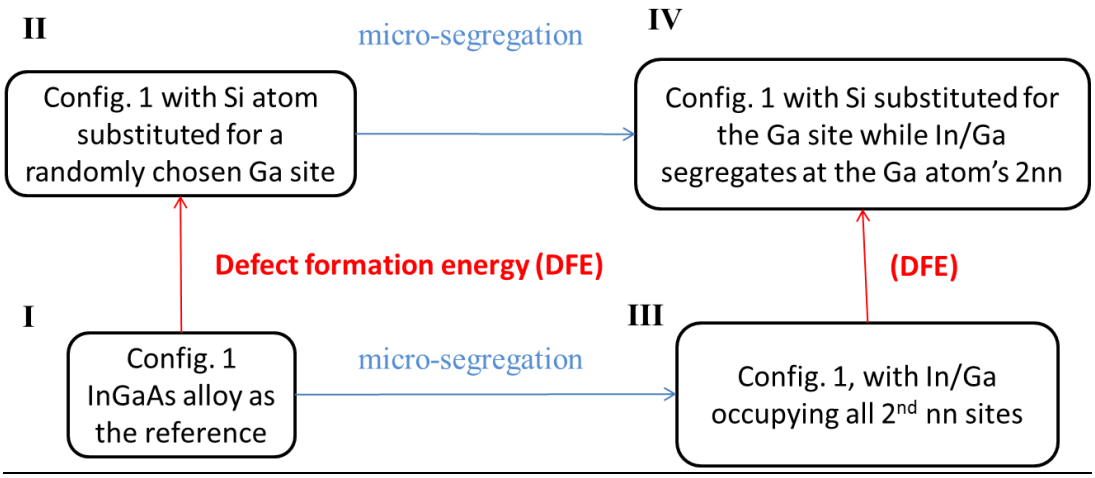

For comparison, we also compare the energy of pure InGaAs of Config.1 (situation I) with the energy of Config.1 InGaAs with micro-segregation of In or Ga for the second nearest neighbors (situation III). This energy difference is defined as the strain energy in this work.

$$E_{strain} = E(III) - E(I)$$

To be more comprehensive, the defect formation energy of different scenarios (from situation I to II *vs.* from III to IV) are also estimated,

CHAPTER 3

Results and Discussion

3.1 Validation of the DFT calculations

Since there is no systematic computational or experimental study of InGaAs alloys, we undertook a verification of the quality of our newly created DFT results. We compared values of the simulated lattice constants of the pure elements (In-In, Ga-Ga, As-As) and thermodynamically stable binary alloys (GaAs and InAs) against known experimental values [6][39][40]. This comparison generally shows good agreement between the DFT and experimental values: The lattice constants agree within a roughly 3% difference in value. More significant differences (typically on the order of 1-2 eV) between our *ab initio* calculations and experimental results were observed for the cohesive energy of covalent bonded elements and binary alloys (Si, As, GaAs and InAs). However, our predicted cohesive energies show very similar results to comparable *ab initio* calculations derived from the MIT-based Materials Project [41]; see the results in Table 6. The tendency of *ab initio* DFT/GGA predictions to overbind structures is well known; see, for example [42]. This difference between experimental results and DFT predictions will be revisited in a later section when we compare our parameters to existing In-Ga-As parameter sets. These existing sets have been shifted by a set amount to match experimental data, as illustrated in Figure 8. Scaling DFT values to match experiment showed no significant difference from using a shifting method [6]. The scaling approach was used here and the accordingly modified parameters that scaling produces are shown in Tables 7 and 8.

Table 6. Comparison of our DFT calculations against experimental data and prior DFT studies

Element/Compound	Properties	Expt. [6][39][40]	DFT/GGA [41]	DFT/GGA (This work)
GaAs (zincblende)	E_{coh} (eV)	6.71	8.4	8.2
	lattice constant (Å)	5.65	5.75	5.76
InAs (zincblende)	E_{coh} (eV)	6.20	7.9	7.7
	lattice constant (Å)	6.06	6.18	6.19
Si (diamond)	E_{coh} (eV)	4.62	5.4	5.4
	lattice constant (Å)	5.43	5.47	5.47
Ga (A11)	E_{coh} (eV)	2.81	3.0	2.9
	a (Å)	4.52	4.57	4.54
	b (Å)	7.66	7.74	7.76
	c (Å)	4.53	4.60	4.61
In (bct)	E_{coh} (eV)	2.52	2.7	2.5
	a (Å)	3.25	3.34	3.31
	c (Å)	4.95	4.94	5.00
As (A7)	E_{coh} (eV)	2.96	4.7	4.7
	a (Å)	4.13	4.17	4.13
	A (deg)	54.12	54.61	55.09

Table 7. Modified parameter sets based on Hammerschmidt [6] after scaling

	Ga-Ga	As-As	In-In	Ga-As	In-As	In-Ga*
D_{ij}(eV)	1.4472	12.774	1.5184	2.3978	2.3408	-
R_{ij}^{0}(Å)	2.3039	1.9330	2.6865	2.4282	2.6091	-
S_{ij}	1.0646	2.3439	1.2440	1.1543	1.8578	-
β_{ij}(1/Å)	0.9079	1.2165	1.1847	1.5396	1.4549	-
γ_{ij}	0.0050	0.3609	0.0109	0.0424	0.0190	⊥
c_{ij}	1.4897	0.1749	1.0853	1.7796	3.9707	⊥
d_{ij}	0.8376	0.2140	0.9465	0.6450	0.9486	⊥
h_{ij}	-0.3373	-0.1261	-0.4652	-0.4060	0.5102	⊥
μ_{ij}(1/Å)	0.7469	2.5408	1.2117	-1.3824	1.1816	⊥
δij	1.4401	4.8650	4.0976	0.2992	2.2113	⊥
nij	1.0	1.0	1.0	1.0	1.0	⊥
mij	1.0	1.0	1.0	1.0	1.0	⊥
R_{ij}^{c}(Å)	2.95	3.1	3.5	3.1	3.7	3.213
D_{ij}^{c}(Å)	0.15	0.1	0.1	0.2	0.1	0.127
As implemented in LAMMPS						
A (eV)	474.067	1545.49	942.511	4552.85	4109.14	668.441
B (eV)	419.365	195.542	437.990	2459.51	260.302	428.576
λ_1 (1/Å)	1.3248	2.6339	1.8687	2.3393	2.8044	1.5868
λ_2 (1/Å)	1.4401	1.1237	1.5021	2.0266	1.5096	1.3733

* The mixing rule proposed by Tersoff [20] can only be used in the form of A,B, λ_1 and λ_2.

⊥These parameters inherit the parent atom's values, *i.e.*, B-A interactions inherit the B atom's values while A-B interactions take over the A atom's values.

Table 8. Modified parameter sets based on Tersoff [18] after scaling

	Si-Si[18]
A (eV)*	3817.1■
B (eV)*	111.51■
λ_1 (1/Å)*	3.2394
λ_2 (1/Å)*	1.3258
$\gamma_{ij}=\beta\perp$	0.33678
c_{ij}	4.8381
d_{ij}	2.0417
h_{ij}	0.0000
$\mu_{ij}=\lambda_3$ (1/Å)$\perp$	1.3258
δij=1$\perp$	Not used
nij	22.956
mij	3.0
R_{ij}^c (Å)	3.0
D_{ij}^c (Å)	0.2

* parameters as defined in eqns. (2) and (3)

■ The Si-Si parameters from [18] were scaled to fit the DFT results in the vertical direction only, by modifying A&B only

$\perp$Different symbols and numbers are used in Tersoff's paper [18]

Figure 8. Schematic to represent shifting the DFT reference data set to match experimental data for equilibrium crystal structures.

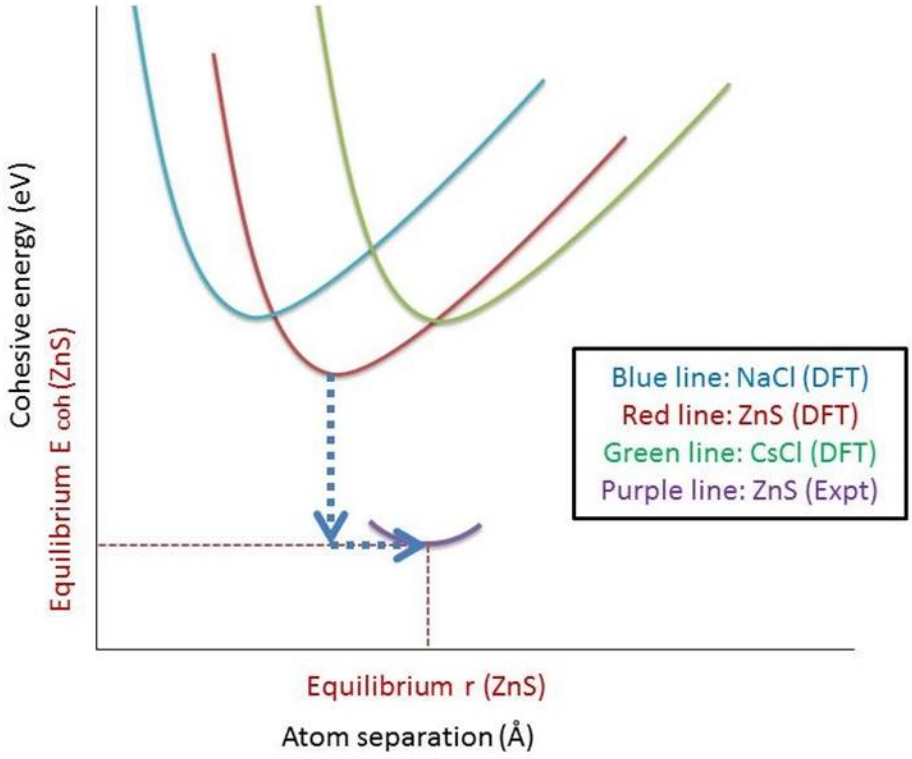

3.2 Validation of Tersoff models against the reference DFT data

Since we fitted our Si-X Tersoff models to a number of different crystal structures, the parameter set that we choose to best represent this ensemble of structures is, of necessity, something of a compromise. Accordingly, the chosen parameter set will not necessarily reproduce all the reference data used in the fitting. Therefore, our first test of the parameter sets for Si-X involves comparing the properties against those calculated from our DFT/GGA reference data set and used in the fitting procedure. As shown in Table 4, values of the bond length and cohesive

energy generated by our Tersoff models agree very well with the DFT results. The average differences between Tersoff predictions and DFT results are small, 0.05-0.06 eV in cohesive energy across the three interactions (Si-As, Ga-Si and In-Si), less than 1% on average, except for h-BN whose properties are compromised in order to get the right trend in defect formation energies when combined with existing In-Ga-As Tersoff models. Even for the NiAs structure (not included in the fitting), the differences are less than 4% across three Si-X interactions. The relative residual error in the DFT results themselves range from 1% (for As) to 9% (for In) [43].

Differences in bond length predictions between Tersoff and DFT are 0.02-0.04 Å, less than 2% on average. This compares well to the relative residual errors in DFT of these constituent atoms of 1-3% [43]. Predictably, the differences in bulk modulus, B, between this Tersoff parameter set and DFT differ more significantly.

The prediction of B requires that the curvature of Energy-Volume space is captured correctly and hence is numerically sensitive. For example, Lejaeghere *et al.* [43] estimate the DFT prediction of B to have a relative residual error against experiment to be 8% for Si, 16% for Ga and In and 35% for As. The average difference between the Tersoff prediction and DFT results for bulk modulus ranges from 3-15 GPa (5-20%) for Si-As, 15-40 GPa (25-70%) for Si-Ga and 5-20 (10-40%) for Si-In. The quality of the fit invariably involves some compromises; for example, if more weight is placed on reproducing the bulk modulus of the ZnS structure, it will usually worsen the reproduction of that of NaCl and CsCl. However, these differences fall within the uncertainty in the DFT results themselves. Overall, then, given that the comparison of DFT to

Tersoff is within recent error predictions for DFT/GGA itself, and that the lattice structures we tested cover a range of structures, some of which are expected arrangements, like zincblende, as well as other rarer structures, this test suggests that the ps.1 and ps.2 parameter sets are acceptably good.

3.3 Prediction of the formation energy of neutral defects

In order to test the transferability of our Tersoff models, we constructed a more stringent test by predicting a property that was *not* included in the fitting process described above. This test is not completely predictive since μ_{ij} was adjusted in order to determine the right *trend* for defect formation energies. As mentioned above, this test also necessitated the creation of a new set of reference DFT data against which to compare the Tersoff predictions. This time, however, the Tersoff results are largely a prediction (barring altering just one parameter, μ_{ij}) and, as such, comparison to our newly generated DFT defect formation energy data is a much stricter test.

As mentioned above, the defect formation of a compound material depends on the chemical potential. Since we only consider neutral defects in this paper, the chemical potential of the electron is ignored ($\mu_e = 0$). For the discussion that follows, we choose conditions that are Si-, Ga-, and In-rich, *i.e.*, $(\mu_{Si} - \mu_{Si}^{Bulk})$=0, $\Delta\mu = \Delta H_f^{InGaAs_2}$ and $\delta\mu$ = 0,

The DFT results predict that the *substitutional* defect that is the most likely to form is one in which Si replaces an In atom in the lattice *(i.e.,* it has the smallest formation energy). However, as we shall show later, this tendency was found to result from the introduction of strain energy induced by having an orderly arrangement of In and Ga atoms on cationic lattice sites. Therefore, as expected, in configuration 1, in which In and Ga atoms are randomly arranged, there is no preference for Si to occupy either an In or a Ga lattice site. On the other hand, for configurations 2 and 3, which have layered structures along certain directions, the substitution of Si on the In site is favored due to the release of strain energy that this allows when a smaller Si atom replaces an In atom. Defects in which Si replaces an anionic As atom in a Ga-rich environment is only 0.2 eV less favored than the case in an In-rich environment.

For situations in which Si atoms occupy *interstitial* locations, our DFT calculations predicted that the formation energies are substantially *higher* than those of substitutional defects. All the interstitial defects in tetrahedral sites give rise to essentially the same formation energy. All the hexagonal interstitial defects are not stable and diffuse back to tetrahedral interstitial sites. The differences among them are generally within the error of the defect formation energy calculations.

The Tersoff-generated and DFT-predicted results of the defect formation energies for a variety of different defects are shown in Table 9. As shown in Table 9 and visualized in Figures 9-14, our first Tersoff parameter set, ps.1, generally predicts a value for the formation energy of the cation substitutional defect that is (a) ~0.1 eV higher than the corresponding DFT calculation, (b)

generally the same order for the formation energy of an anion substitutional defect, and (c) ~1.3 eV lower for the energies of the T1 interstitial defects. The T2 interstitial defects, described in section 2.3.3, were the least well predicted, generally ~3.5 eV higher than their DFT counterparts for the defect formation energies. This tendency for Tersoff models to predict higher formation energies is well known. For example, similar studies for GaAs [44] show that differences of 0.5-3.0 eV between DFT and Tersoff values are not uncommon. In comparison, the ps.2 parameter sets (by design) predict a value ~0.4 eV lower for the formation energy of the cationic substitutional defects than the corresponding DFT calculations. Since the anionic defect formation energy is controlled by the Si-Ga and Si-In interactions, which are identical for ps.1 and ps.2, its value is the same for both parameter sets. The defect formation energies predicted by ps.2 are ~1.6 eV lower for T1 interstitial defects and ~0.9 eV lower for T2 interstitial defects than corresponding DFT calculations.

Echoing the DFT results, ps.1 also predicts that the substitutional defect in which Si replaces In is the most energetically favorable substitution, but the Tersoff model has a systematic preference for the anionic substitutional defect of ~0.05 eV. On the other hand, although ps.2 has a systematic preference for the cationic substitutional defect by ~0.45 eV, it still predicts that substitutional defects in which Si replaces In are the most energetically favorable change. For the comparison between interstitial and substitutional defects, both ps.1 and ps.2 predict that Si dopants occupying interstitial lattice sites are substantially less energetically favored compared to Si dopants on substitutional lattice sites.

The ps.1 parameter set, which predicts the right trend across all the defect categories and configurations, was thus shown to be able to likely to find the most probable local environments around Si in a host InGaAs matrix.

Table 9. Formation energy of neutral defects from *ab initio* and Tersoff models

Defect	Config. 1 GGA/ps.1/ ps.2	Config. 2	Config.3
*Substitutional defect*s			
Si_{Ga} (Si on a Ga site)	0.96/1.12/0.57 eV	0.98/1.12/0.59	0.98/1.22/0.58
Si_{In} (Si on an In site)	0.98/0.95/0.47	0.52/0.69/0.15	0.73/0.78/0.38
Si_{As} (Si on an As site)	0.90/0.87/0.87 (2Ga2In)	0.69/0.83/0.83 (3Ga1In) 0.89/1.00/1.00 (1Ga3In)	0.88/0.89/0.89 (2Ga2In)
Interstitial Si			
Si_{T1}^{*} (Si atom in a tetrahedral, T1, site)	3.24/1.43/1.44 (3Ga3In)	3.02/1.50/1.54 (3Ga3In)	3.02/1.99/1.90 (4Ga2In) 3.12/2.42/1.22 (2Ga4In)
Si_{T2}^{**} (Si atom in a tetrahedral, T2, interstitial site)	3.30/7.77/2.48 (2Ga2In)	2.97/5.78/1.43 (3Ga1In) 3.23/6.47/2.57 (1Ga3In)	3.17/6.77/2.47 (2Ga2In)

Figure 9. Energy differences between predictions of the Tersoff potential models and our DFT calculations for defect formation energies. Results are shown for our two sets of Tersoff parameters (ps.1 and ps.2) and for four defect categories: cationic and anionic substitutional sites (blue and red, respectively) and for two types of interstitials, T1 and T2 (green and purple, respectively). Ps.1 performs better at predicting defect formation energies from substitutional sites; ps.2 is substantially better at predicting T2-type interstitials, but performs slightly worse for the substitutional sites

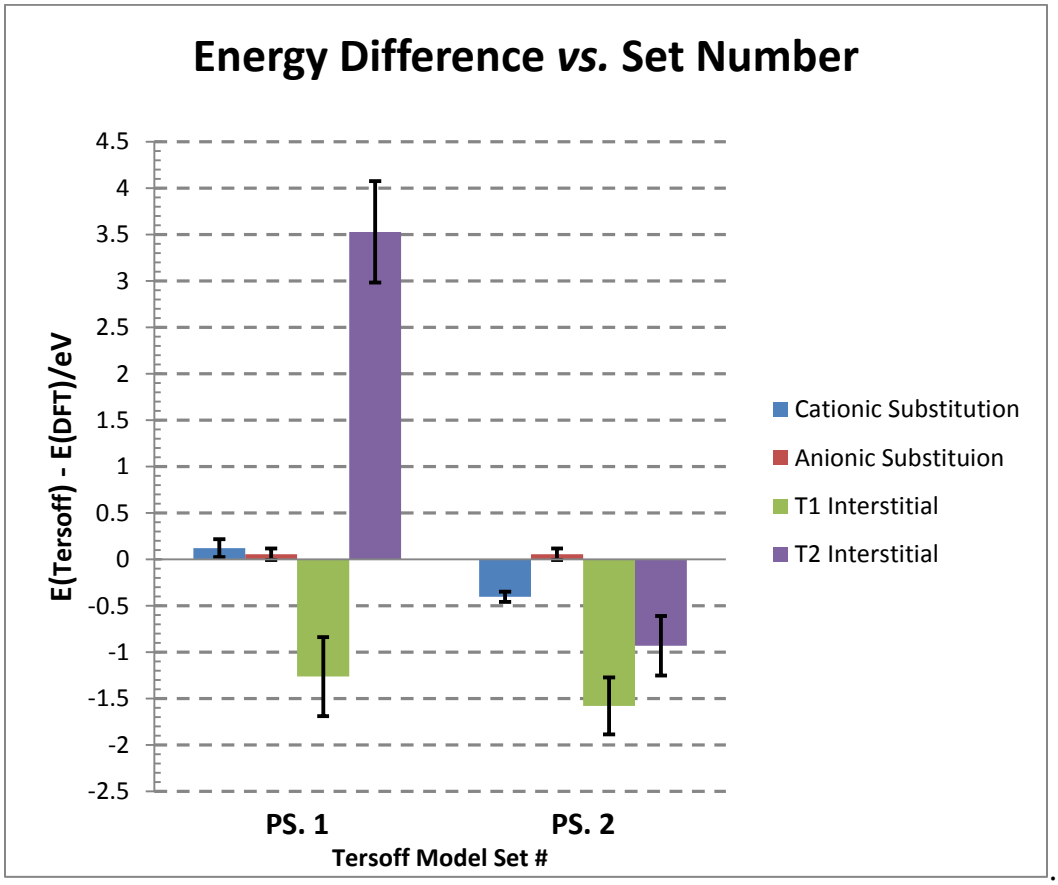

Figure 10. Scatter charts of Tersoff-generated defect formation energy against DFT- generated defect formation energy values. Parameter set 1 (red dots) predicts a better trend for substitutional defects, while parameter set 2 (green dots) predict a better trend for interstitial defects.

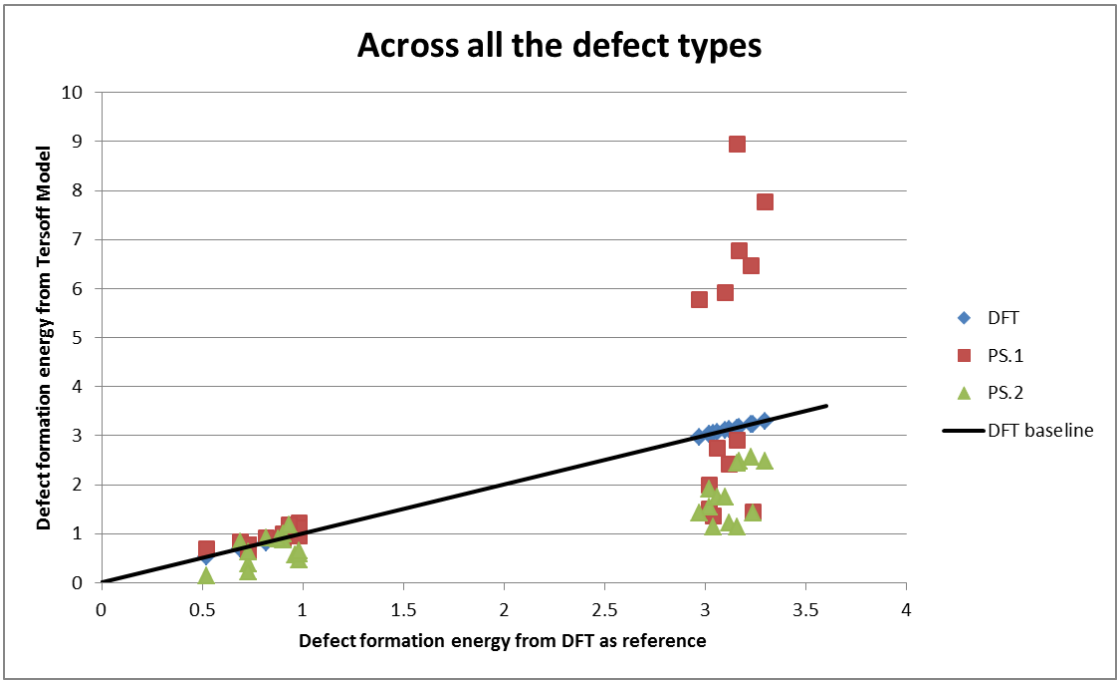

Figure 11. Scatter chart for cationic substitutional defects only. Both ps. 1 and ps. 2 show the right trends, but the values predicted by ps.1 are closer to the DFT values.

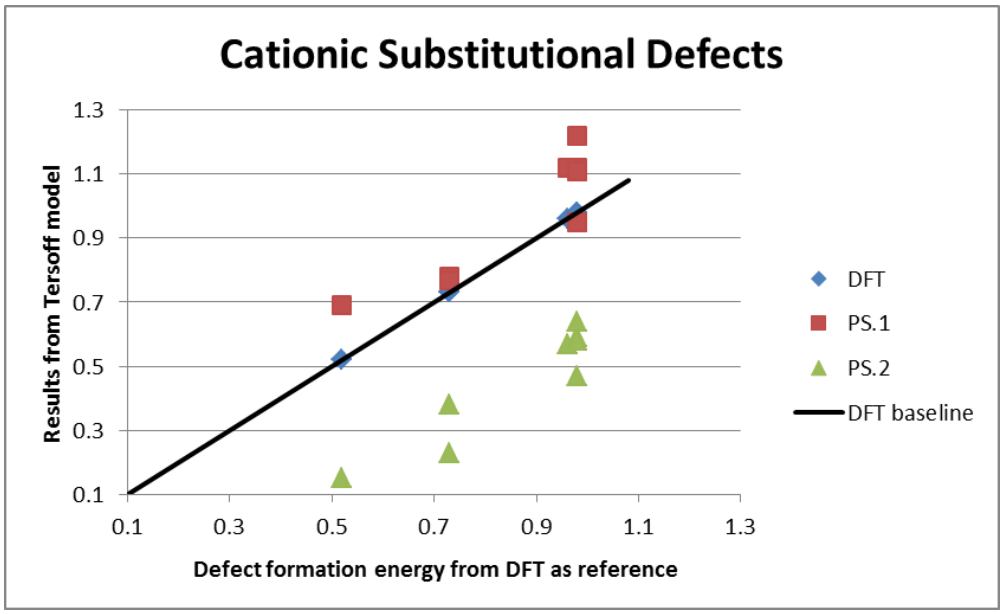

Figure 12. Scatter chart for anion substitutional defects only. Since anion substitution is controlled by Si-Ga and Si-In interactions which are the same for ps. 1and 2., both parameter sets share the same result.

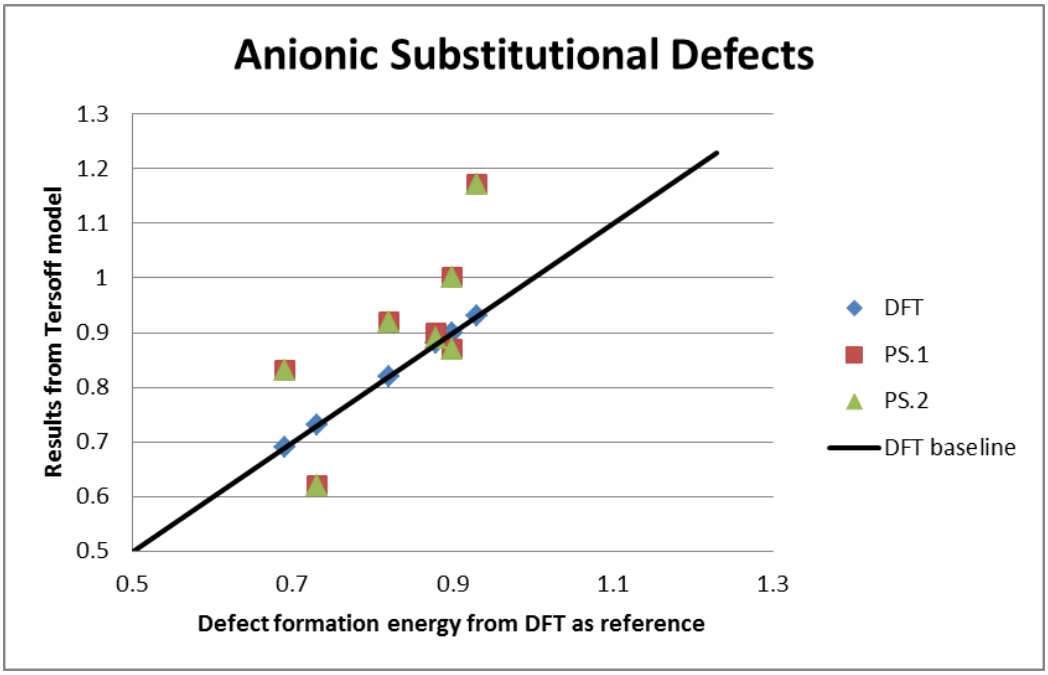

Figure 13.Scatter chart for T1 interstitial defects only. Neither ps. 1 nor ps.2 follow the trend of DFT-generated values. However, they both predict higher values for interstitial defect formation energies than for substitutional defects.

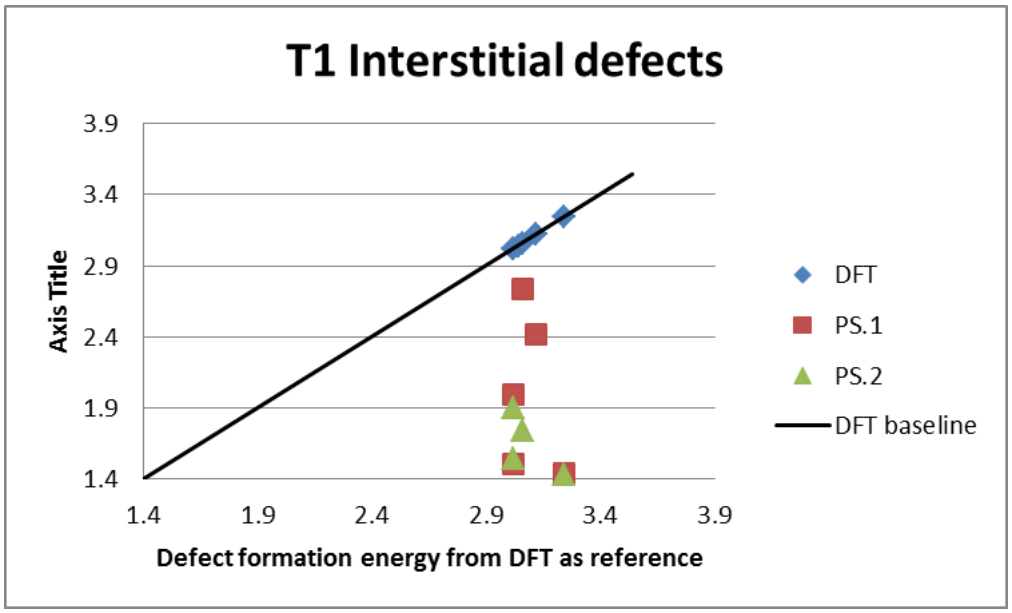

Figure 14. Scatter chart for T2 interstitial defects only. Both ps. 1 and ps. 2 predict higher values for interstitial defects compared to substitutional ones, but values predicted by ps.1 are far higher than DFT-generated values.

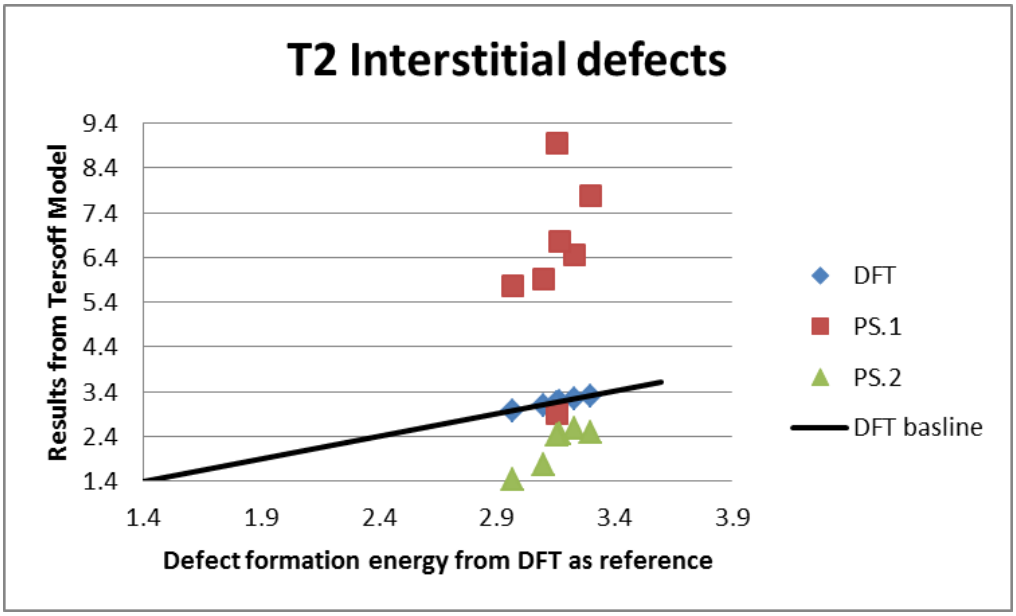

3.4 Micro-segregation of In/Ga

Since the Tersoff models developed in this work were shown to be capable of an acceptably accurate representation of the DFT results and, by extension, to be likely to offer constructive information regarding identifying the most probable local environments around Si dopants in InGaAs alloys, we were able to begin to test our hypothesis that Si atom will prefer to reside on certain lattice sites due to its corresponding local environment.

This hypothesis was tested by comparing the defect formation energy that results from substituting a Si atom for a Ga site in Config.1 and then altering the nature of its immediate environment (2^{nd} nearest neighbor). Thus, we take a randomly substituted $In_{0.50}Ga_{0.50}As$ alloy (Config. 1) and make a Si substitution for a Ga site. Then we study the effect of what might be termed local "micro-segregation" by altering the In/Ga ratio of the 12 second-nearest neighbors of the chosen Ga site. For this test, we chose to use two extreme cases in which all 12 2^{nd} nearest neighbors are either In or Ga atoms. The energies of both these environments, compared to a completely random arrangement of In/Ga 2^{nd} nearest neighbors will then provide information about the effects of micro-segregation on the ability of Si defects to form.

The results shown in Table 10 show that even this extreme micro-segregation of In/Ga will not affect the resultant defect formation energy; the difference in formation energies across all the columns is within the intrinsic uncertainty of 0.1~0.2 eV. However, micro-segregation will

introduce considerable strain energy into the system. Comparing the values on rows 2 and 3 of Table 10, we can see that there is no significant difference in formation energies, leading to the conclusion that micro-segregation will only introduce strain energy to the system, but will not make alter the preference for the choice of lattice site, In or Ga.

Echoing the DFT results shown in the previous section, although micro-segregation of cations around a dopant atom will not affect the defect formation energy, local ordering of In or Ga can make In cationic lattice sites favored due to the release of strain energy. While this refutes our initial hypothesis, it introduces a new concept into the problem, namely the nature of any ordering in InGaAs alloys.

Table 10. Strain energies and defect formation energies for the pathways illustrated in Figure 7 of Chapter 2. The effect of strain energy introduced by micro-segregation is shown in rows two (I → III) and three (II→IV). The data show that strain energy is significant. The effect of the defect formation energy is shown in row four (I→II and III→IV). Results show that defect formation energy is the same in random (column 1) and micro-segregated environments (columns 2 and 3). The first row shows the energy differences compared to the reference situation I. It can be seen that the sum of the strain and formation energies (rows 2 or 3 with row 4) is essentially the same as that in row 1.

4096-atom box	Config. 1	Ga segregation at 2^{nd} nn	In segregation at 2^{nd} nn
I →II or IV	1.10 eV	2.65	1.83
I → III	0.00 eV (reference)	+1.64 eV	+0.78 eV
II → IV	0.00 eV	+1.55 eV	+0.73 eV
I → II (III → IV)	1.10 eV	1.01eV	1.05 eV

CHAPTER 4

Conclusions

The major products from this work are the semi-empirical Tersoff models developed for Si-X interactions (X = In, Ga, As), an *ab initio* database for bulk structural properties of the Si-X "compounds" (Si-Ga and Si-In being theoretical alloys) and for the extrinsic defect formation energies of a dopant in a $In_{0.5}Ga_{0.5}As$ alloy. These databases can act as the (reference) comparison group for further studies of dopant activation in InGaAs alloys.

Two sets of Tersoff parameters have been developed to represent Si-X interactions (where X= Ga, In, As); these sets differ in the weighting placed on the influence of different crystal structures in the fitting process. Both parameter sets, shown in Table 3, represent a 'best fit' to a range of crystal structures. They show strong consistency with the DFT/GGA reference data set for at least zincblende and rock salt structures, with results mostly within the known intrinsic errors of the DFT/GGA method itself. Overall, the errors of our Tersoff model are less than 1% for cohesive energy, less than 2% for bond length and less than 30% for most of the bulk modulus values.

Parameter set ps.1 shows formation energies for cationic and anionic substitutional defects that are very close to DFT/GGA predictions, at the expense of a poorer prediction of some interstitial defects. Generally speaking, ps.1 has the ability to predict the right trend among different categories of defects and within substitutional defects. The alternative parameter set, ps.2,

obtained by developing a new Si-As interaction with an adjusted μ_{ij} (but leaving the Si-Ga and Si-In potentials unchanged from ps.1) is substantially better at predicting T2-type interstitials, but does slightly worse in predicting the formation energies of substitutional sites. For the simulation of kinetic properties, the ps.2 parameter set might be a more judicious choice due to its improved reproduction of the interstitial defects relative to ps.1.

The study on micro-segregation shows that, for extreme cases in which all the 2nd nearest neighbors of a dopant are all the same type of cation (In or Ga), this will introduce significant strain energy into the system, *i.e.*, thermodynamically less favored, in which Si will prefer to sit on In sites. However, even these extreme micro-segregation environments do not affect the defect formation energy, thus making neither cation lattice site (In or Ga) preferred. The effect of less extreme cases on the strain energy has not been explored, but would be an interesting future study. These results partially negate our original hypothesis that the local environment affected the defect formation energy, but they provide another way to approach the problem by investigating how In and Ga atoms are arranged in InGaAs alloys and hence allowing an assessment of the extent of strain in the system and its influence on dopant diffusion and hence activation.

Overall, while the correspondence between Tersoff and DFT/GGA predictions of the sensitive defect formation energies differs from situation to situation, they are similar to the kinds of results that are typically found by others when comparing Tersoff models to DFT calculations. Our results suggest that the first set of Tersoff parameters (ps.1) we constructed should work

well for finding the most probable local environment around Si, but its over-prediction of the formation energy of the T2 interstitial defect may deleteriously affect its ability to predict the migration energy and other kinetic properties. However, to quote Murdick's assessment of the Tersoff model to predict defect formation energy predictions in GaAs: "For a wide range of processing conditions, there is no potential that is clearly superior [to Tersoff]."

CHAPTER 5

Future work

The ps.1 Tersoff model set developed in this work not only passes the validation test to reproduce the reference data, but also survived the more stringent test to predict the right trend across the matrix of different defect categories and InGaAs configurations with different local environments. Therefore, ps.1 Tersoff model appears to be capable of finding the most probable local environment around Si dopant in InGaAs alloy.

Preliminary studies on the effect of micro-segregation at the second nearest neighbors of cation sites did not give promising results for our hypothesis, but the role of a proximal vacancy in this hypothesis has not yet been studied. The results of micro-segregation also provide an incentive to use a Monte Carlo method, combined with the Tersoff models developed in this work and existing In-Ga-As Tersoff models, to study the arrangement of In and Ga atoms in InGaAs alloy, and how the arrangement of the atoms (In, Ga, As) affects the strain in the system and how that will affect the best composition ratio of In over Ga.

In addition to the original motivation of this work, the Tersoff models developed in this work can be further tested for transferability by predicting the migration energy of Si defects in InGaAs alloys using the nudged elastic band (NEB) method. It would also be possible to run Molecular Dynamics simulations of Si dopants in InGaAs.

Besides exploiting the power of the models developed in this work, a more comprehensive study of the formation energy of charged defects using DFT should provide us more insights about the stability of defects and their dependences on the Fermi level. This is particularly important to study since, in practice, defects are usually charged.

Furthermore, experimental data from Raman studies of Si-doped InGaAs samples have been acquired by our collaborators, but the meaning (identification) of some critical peaks in the spectra still remain unknown. If possible, a DFT/Tersoff-generated Raman spectrum would be an instructive way to identify these peaks and therefore provide another source of information that will help us understand Si dopant activation in InGaAs alloys.

Ultimately, these approaches will provide an understanding of the energy landscape as a function of the local environment of dopants. This, in turn, will suggest ways to understand the nature of Si dopant activation in InGaAs alloys and direct studies that explore the advantages of laser spike annealing (LSA) for ternary III-V alloys.

REFERENCES

[1] P. Clarke, “Intel’s Gargini pushes III-V-on-silicon as 2015 transistor option,” *EE Times*, 2010. [Online]. Available: http://www.eetimes.com/document.asp?doc_id=1173048. [Accessed: 09-Apr-2014].

[2] J. W. Wagner, “Preparation and Properties of Bulk In[sub 1−x]Ga[sub x]As Alloys,” *J. Electrochem. Soc.*, vol. 117, no. 9, p. 1193, Sep. 1970.

[3] J. C. Woolley, M. B. Thomas, and A. G. Thompson, “Optical energy gap variation in Ga x In 1− x As alloys,” *Can. J. Phys.*, vol. 46, no. 2, pp. 157–159, Jan. 1968.

[4] “International Technology Roadmap for Semiconductors 2012 Update Overrview,” *ITRS*, 2012. [Online]. Available: http://www.itrs.net/Links/2012ITRS/2012Chapters/2012Overview.pdf. [Accessed: 09-Apr-2014].

[5] S. J. Pearton, J. M. Kuo, W. S. Hobson, E. Hailemarian, F. Ren, A. Katz, and A. P. Perley, “Ion Implantation Doping of InGaP, InGaAs, and InAlAs,” *MRS Online Proc. Libr.*, vol. 240, 1991.

[6] T. Hammerschmidt, P. Kratzer, and M. Scheffler, “Analytic many-body potential for InAs/GaAs surfaces and nanostructures: Formation energy of InAs quantum dots,” *Phys. Rev. B*, vol. 77, no. 23, 2008.

[7] E. Schrödinger, “An Undulatory Theory of the Mechanics of Atoms and Molecules,” *Phys. Rev.*, vol. 28, no. 6, pp. 1049–1070, Dec. 1926.

[8] J. C. Slater, “A simplification of the Hartree-Fock method,” *Phys. Rev.*, vol. 81, pp. 385–390, 1951.

[9] C. Møller and M. S. Plesset, “Note on an Approximation Treatment for Many-Electron Systems,” *Phys. Rev.*, vol. 46, no. 7, pp. 618–622, Oct. 1934.

[10] C. W. Bauschlicher, S. R. Langhoff, P. R. Taylor, and H. Partrigge, “A full CI treatment of Ne atom - a benchmark calculation performed on the NAS CRAY 2,” *Chem. Phys. Lett.*, vol. 126, no. 5, pp. 436–440, May 1986.

[11] D. Maurice and M. Head-Gordon, “Analytical second derivatives for excited electronic states using the single excitation configuration interaction method: theory and application to benzo[a]pyrene and chalcone,” *Mol. Phys.*, vol. 96, no. 10, pp. 1533–1541, May 1999.

[12] N. Metropolis, A. W. Rosenbluth, M. N. Rosenbluth, A. H. Teller, and E. Teller, “Equation of State Calculations by Fast Computing Machines,” *J. Chem. Phys.*, vol. 21, no. 6, p. 1087, Dec. 1953.

[13] E. Pollock and D. Ceperley, “Simulation of quantum many-body systems by path-integral methods,” *Phys. Rev. B*, vol. 30, no. 5, pp. 2555–2568, Sep. 1984.

[14] P. Hohenberg, “Inhomogeneous Electron Gas,” *Phys. Rev.*, vol. 136, no. 3B, pp. B864–B871, Nov. 1964.

[15] W. Kohn and L. J. Sham, “Self-Consistent Equations Including Exchange and Correlation Effects,” *Physical Review*, vol. 140, no. 4A. pp. A1133–A1138, 1965.

[16] K. Capelle, “A bird’s-eye view of density-functional theory,” p. 69, Nov. 2002.

[17] H. J. Monkhorst and J. D. Pack, “Special points for Brillouin-zone integrations,” *Phys. Rev. B*, vol. 13, no. 12, pp. 5188–5192, Jun. 1976.

[18] J. Tersoff, “New empirical approach for the structure and energy of covalent systems,” *Physical Review B*, vol. 37. pp. 6991–7000, 1988.

[19] J. Tersoff, “Empirical interatomic potential for silicon with improved elastic properties,” *Phys. Rev. B*, vol. 38, pp. 9902–9905, 1988.

[20] J. Tersoff, “Modeling solid-state chemistry: Interatomic potentials for multicomponent systems,” *Phys. Rev. B*, vol. 39, no. 8, pp. 5566–5568, 1989.

[21] R. Smith, “A semi-empirical many-body interatomic potential for modelling dynamical processes in gallium arsenide,” *Nucl. Instruments Methods Phys. Res. Sect. B Beam Interact. with Mater. Atoms*, vol. 67, no. 1–4, pp. 335–339, Apr. 1992.

[22] M. Sayed, J. H. Jefferson, A. B. Walker, and A. G. Cullis, “Molecular dynamics simulations of implantation damage and recovery in semiconductors,” *Nucl. Instruments Methods Phys. Res. Sect. B Beam Interact. with Mater. Atoms*, vol. 102, no. 1–4, pp. 218–222, Aug. 1995.

[23] P. A. Ashu, J. H. Jefferson, A. G. Cullis, W. E. Hagston, and C. R. Whitehouse, “Molecular dynamics simulation of (100)InGaAs/GaAs strained-layer relaxation processes,” *J. Cryst. Growth*, vol. 150, pp. 176–179, May 1995.

[24] K. Nordlund, J. Nord, J. Frantz, and J. Keinonen, “Strain-induced Kirkendall mixing at semiconductor interfaces,” *Comput. Mater. Sci.*, vol. 18, no. 3–4, pp. 283–294, Sep. 2000.

[25] D. Powell, M. Migliorato, and A. Cullis, “Optimized Tersoff potential parameters for tetrahedrally bonded III-V semiconductors,” *Phys. Rev. B*, vol. 75, no. 11, p. 115202, Mar. 2007.

[26] H. Detz and G. Strasser, “Modeling the elastic properties of the ternary III–V alloys InGaAs, InAlAs and GaAsSb using Tersoff potentials for binary compounds,” *Semicond. Sci. Technol.*, vol. 28, no. 8, p. 085011, Aug. 2013.

[27] J. Tersoff, “New empirical model for the structural properties of silicon,” *Physical Review Letters*, vol. 56. pp. 632–635, 1986.

[28] O. Madelung, U. Rössler, and M. Schulz, Eds., *Non-Tetrahedrally Bonded Elements and Binary Compounds I*, vol. 41C. Berlin/Heidelberg: Springer-Verlag, 1998.

[29] J. P. Perdew, K. Burke, and M. Ernzerhof, “Generalized Gradient Approximation Made Simple,” *Phys. Rev. Lett.*, vol. 77, no. 18, pp. 3865–3868, Oct. 1996.

[30] R. Biswas and D. Hamann, “Interatomic Potentials for Silicon Structural Energies,” *Physical Review Letters*, vol. 55. pp. 2001–2004, 1985.

[31] “Computer Graphic Service (Genplot).” [Online]. Available: http://www.genplot.com/. [Accessed: 04-May-2014].

[32] K. Albe, K. Nordlund, J. Nord, and A. Kuronen, “Modeling of compound semiconductors: Analytical bond-order potential for Ga, As, and GaAs,” *Phys. Rev. B*, vol. 66, no. 3, p. 035205, Jul. 2002.

[33] P. Giannozzi, S. Baroni, N. Bonini, M. Calandra, R. Car, C. Cavazzoni, D. Ceresoli, G. L. Chiarotti, M. Cococcioni, I. Dabo, A. Dal Corso, S. de Gironcoli, S. Fabris, G. Fratesi, R. Gebauer, U. Gerstmann, C. Gougoussis, A. Kokalj, M. Lazzeri, L. Martin-Samos, N. Marzari, F. Mauri, R. Mazzarello, S. Paolini, A. Pasquarello, L. Paulatto, C. Sbraccia, S. Scandolo, G. Sclauzero, A. P. Seitsonen, A. Smogunov, P. Umari, and R. M. Wentzcovitch, “QUANTUM ESPRESSO: a modular and open-source software project for quantum simulations of materials.,” *J. Phys. Condens. Matter*, vol. 21, p. 395502, 2009.

[34] F. D. Murnaghan, “The Compressibility of Media under Extreme Pressures.,” *Proc. Natl. Acad. Sci. U. S. A.*, vol. 30, no. 9, pp. 244–7, Sep. 1944.

[35] J. Northrup, “Energetics of GaAs island formation on Si(100),” *Phys. Rev. Lett.*, vol. 62, no. 21, pp. 2487–2490, May 1989.

[36] S. Zhang and J. Northrup, “Chemical potential dependence of defect formation energies in GaAs: Application to Ga self-diffusion,” *Physical Review Letters*, vol. 67. pp. 2339–2342, 1991.

[37] J. Northrup and S. Zhang, “Dopant and defect energetics: Si in GaAs,” *Physical Review B*, vol. 47. pp. 6791–6794, 1993.

[38] S.-G. Lee and K. J. Chang, “Energetics and hydrogen passivation of carbon-related defects in InAs and In0.5Ga0.5As,” *Phys. Rev. B*, vol. 53, no. 15, pp. 9784–9790, Apr. 1996.

[39] C. Kittel, *Introduction to Solid State Physics*, vol. 10. 2005, p. 680.

[40] *Handbook of Semiconductor Silicon Technology*. Noyes Publications, 1990, p. 795.

[41] A. Jain, G. Hautier, S. Ong, C. Moore, C. Fischer, K. Persson, and G. Ceder, "Formation enthalpies by mixing GGA and GGA + U calculations," *Physical Review B*, vol. 84. 2011.

[42] S. Sanvito, G. Theurich, and N. A. Hill, "Density Functional Calculations for III–V Diluted Ferromagnetic Semiconductors: A Review," *J. Supercond.*, vol. 15, no. 1, pp. 85–104, Feb. 2002.

[43] K. Lejaeghere, V. Van Speybroeck, G. Van Oost, and S. Cottenier, "Error Estimates for Solid-State Density-Functional Theory Predictions: An Overview by Means of the Ground-State Elemental Crystals," *Crit. Rev. Solid State Mater. Sci.*, vol. 39, no. 1, pp. 1–24, Jan. 2014.

[44] Dewey Andrew Murdick, "Simulating the Atomic Assembly of Gallium Arsenide," University of Virginia, 2006.